STARS

2012

Simulation Of Heat/mass Transfer Of A Three-layer Impingement/effusion Cooling System

Brandon Smith
University of Central Florida

University of Central Florida

Showcase of Text, Archives, Research & Scholarship

SIMULATION OF HEAT/MASS TRANSFER OF A THREE-LAYER IMPINGEMENT/EFFUSION COOLING SYSTEM

by

BRANDON E. SMITH
B.S. University of Central Florida, 2012

A thesis submitted in partial fulfillment of the requirements
for the degree of Master of Science in Mechanical Engineering
in the Department of Mechanical, Materials, and Aerospace Engineering
in the College of Engineering and Computer Science
at the University of Central Florida
Orlando, Florida

Fall Term
2012

ABSTRACT

Cooling techniques for high density electrical components and electronic devices have been studied heavily in recent years. The advancements in the electrical/electronic industry have required methods of high heat flux removal. Many of the current electrical components and electronic devices produce a range of heat fluxes from 20 W/cm^2 – 100 W/cm^2. While parallel flow cooling systems have been used in the past, jet impingement is now more desirable for its potential to have a heat transfer coefficient 3-5 times greater than that of parallel flow at the same flow rate. Problems do arise when the jet impingement is confined and a cross flow develops that interacts with impinging jets downstream leading to a decrease in heat transfer coefficient. For long heated surfaces, such as an aircraft generator rotor, span wise fluid management is important in keeping the temperature distribution uniform along the length of the surface. A detailed simulation of the heat/mass transfer on a three-layer impingement/effusion cooling system has been conducted. The impingement jet fluid enters from the top layer into the bottom layer to impinge on the heated surface. The spent fluid is removed from the effusion holes and exits through the middle layer. Three different effusion configurations were used with effusion diameters ranging from 0.5 mm to 2 mm. Temperature uniformity, heat transfer coefficients, and pressure drops were compared for each effusion diameter arrangement, jet to target spacing (H/d), and rib configuration. A Shear Stress Transport (SST) turbulence fluid model was used within ANSYS CFX to simulate all design models. Three-layer configurations were also set in series for long, rectangular heated surfaces and compared against traditional cooling methods such as parallel internal flow and traditional jet impingement models. The results show that the three-layer design compared to a traditional impingement cooling scheme

over an elongated heated surface can increase the average heat transfer coefficient by 75% and reduce the temperature difference on the surface by 75%. It was shown that for a three layer design under the same impingement geometry, the average heat transfer coefficient increases when H/d is small. The inclusion of ribs always provided better heat transfer and centralized the cooling areas. The heat transfer was increased by as much as 25% when ribs were used. The effusion hole arrangement showed minimal correlation to heat transfer other than a large array provides better results. The effusion holes' greatest impact was found in the pressure drop of the cooling model. The pressure losses were minimal when the effective area of effusion holes was large. This minimizes the losses due to contraction and expansion.

ACKNOWLEDGMENTS

Every chapter in one's life is meant to build character. The ones that build the most character sometimes bring the most challenges. This research is testament to that truth in my life. The time spent collecting data, modifying models, and pouring over journals was exhaustive but it confirmed engineering as my lifelong profession. I am thankful to my advisor, Dr. Louis Chow, for his guidance and patience during the entire process. This journey would not have been possible without his willingness to accept me as a researcher. I am blessed to have had a great support of friends, family, and fellow researchers that have given advice when it was needed. Finally, I thank God for the grace he has shown me and the peace he has given me, a peace that surpasses all understanding.

TABLE OF CONTENTS

LIST OF FIGURES

LIST OF TABLES

NOMENCLATURE

CFD $\qquad$ = computational fluid dynamics

d $\qquad$ = jet nozzle diameter

d_{eff} $\qquad$ = effusion hole diameter

d_h $\qquad$ = hydraulic diameter

f $\qquad$ = friction factor

G_c $\qquad$ = cross-flow mass velocity based on channel cross-sectional area

G_j $\qquad$ = jet mass velocity based on jet hole area

h $\qquad$ = heat transfer coefficient

H, z $\qquad$ = jet-to-target height

I $\qquad$ = electrical current

K $\qquad$ = thermal conductivity of the fluid

K $\qquad$ = minor loss coefficient

Nu $\qquad$ = Nusselt number

PAO $\qquad$ = poly-alpha-olephin

Pr $\qquad$ = Prandtl number

q'' $\qquad$ = heat per unit area

R = electrical resistance

Re = Reynolds number

s = jet-to-jet spacing

T_{in} = inlet temperature

T_{max} = maximum temperature on the heated surface

T_{min} = minimum temperature on the heated surface

T_s = surface temperature

$\overline{V}$ = mean velocity in a pipe

x_n = stream-wise jet hole spacing

y_n = span-wise jet hole spacing

CHAPTER 1 - INTRODUCTION

The volume and complexity of electronic devises is ever increasing in today's society. Electricity has long since established itself as a major, if not the most important, form of usable energy to power all that we come in contact with. Trains, planes, and automobiles; houses, hotels, and apartment complexes; phones computers and micro devises all require electricity to function. What is more is that the current demand is not for bigger and better but smaller and more efficient; smaller and more powerful. Many advances in the field of super conductors and micro chips are allowing this to happen but behind all these devises lay a part of physics that cannot be ignored; these devices are not 100% efficient. While we try to maximize all that we can many physical laws governing our devices along with the deficiencies in our materials and processes will not allow us to use every bit of power harnessed. So where do these percentages of loss go? Are the losses something that needs to be dealt with or can they be left alone? We have all experienced a laptop that has been running a long time. The internal parts generate heat. Under many circumstances we must either let it cool down by turning it off or find an effective way to cool the machine. It is intuitive knowing that if a computer over heats it will not perform correctly or even worse will break down. We just discovered two principles behind all electronic devices; that electric loads in any device produce heat, I^2R losses, and when the heat is miss managed or above design specifications parts begin to fail due to undesired temperatures. We can see the effects electric loads have on a laptop computer but what happens when the electric loads are higher and the devices are more demanding? Cooling for electronic devices has been and is continuing to be an important topic when discussing the development of high density

electronic devises that have heat fluxes ranging from 23-100 W/cm^2. Common fields of study in cooling for high density electronic devices are cooling fluid properties, flow management, cooling geometries as well as specific functions the cooling device is used for. While most cooling systems are geared towards electronic devices similar cooling schemes are used in other areas of engineering such as turbine blade cooling. The thermal and fluid dynamics are the same just assigned different applications. A highly effective cooling method in this field of study utilizes jet impingement onto a heated surface. A single fluid jet or an array of such jets, impinging normally on a surface, may be used to achieve enhanced coefficients for convective heating, cooling, or drying. While simple jet impingement geometries and flow schemes are easily predicted through equations based on key parameters many flow schemes are based off complicated geometries that are much more difficult to predict. For example an array of jets along a long surface where jet to jet interaction occurs can cause variance in heat transfer coefficients, many times undesirable, and needs to be solved through experimental design or numerical simulations. With the advancement of computing power and computational fluid modeling numerical simulation have become an advantageous way to model flow geometries and the thermal impact a cooling scheme can have under certain boundary conditions. Specifically for this work a cooling scheme under the geometrical constraints and heat loads of an aircraft generator rotor winding is to be modeled and simulated to find a desirable cooling system that will provide adequate temperature profiles and flow management.

CHAPTER 2 - LITERATURE REVIEW

The following chapter will present an all-encompassing review of relevant literature and theory linked with the methodology and analysis presented in the following content of this work. First will be a summary of aircraft generator cooling and the methods of cooling used followed by an extensive look jet impingement and the effects certain parameters have on the thermal coefficients associated with jet impingement. Cooling models utilizing similar geometries and flow properties as the present work will be used to create a baseline for modeling. Finally, comparisons of numerical fluid modeling and computational fluid dynamic used will be presented.

Aircraft Generator Cooling

Aircraft generators are powered by an aircraft's turbine engine and the physical size of each generator is dependent on the amount of power, volt-amps (VA), output of the generator. With increasing electric demands for the same size generator the electric loadings for stator and rotor windings are increasing. King [1] sought to find a feasible internally wetted generator cooling system due to the recent appearance of high temperature, fluid resistant film insulations. A study was initiated to re-examine and evaluate further potential advantages which might accrue to direct oil cooling by internal spray techniques. With promising results a program for development was initiated and presented a large number of spray oil-cooled generators. What was found was that both rotor and stator conduction cooling portions were ineffective, stationary spray nozzles on the stator were also relatively ineffective, but most effective cooling method

appeared to be one with a limited number of large diameter nozzles on the rotor with an optimal

nozzle size of 0.033 in. in diameter. US Patent 3,659,125 [2] is one of the nozzle schemes used

on the rotor that allowed the oil to spray onto the winding only by the rotational force from the

rotor spinning. Also documented was that the rotor winding temperatures were limited by the

coking tendencies of the oil and not by the temperature limitation of the insulations. Between the

1950s and 1970s integrated drive generators emerged as effective equipment in industry for

improving power/weight ratios of aircraft generators. These generators elegantly harnessed the

advantages of the direct liquid-cooled generator. Kennett [3] describes in detail the components,

configuration, and materials used in an i.d.g. assembly. More specifically detailed is the working

fluid flow loop. The synthetic turbine oil is fed by a charge pump both to the hydraulic circuits

and through the a.c. generator frame. The oil in the fame is transferred into the shaft where a

portion is diverted through a metering annulus and lubricates the bearing before passing under

the influence of centrifugal force over adjacent end windings. Oil thrown from various rotor

surfaces also passes over the stationary windings before draining into the sump pumps located

within the i.d.g frame. Scavenge pumps extract this drainage from the a.c. generator windings

and return the oil to the hydraulic system. Gasperetti [4] also found that spray oil cooling would

provide weight reduction, enhance generator reliability, and lengthen overhaul intervals. Detail

was provided for inlet fluid temperatures, fluid temperature rise through the generator, and

required oil pressures for specific designs. Most notably a comparison of oil to air use was given

and showed the rise in oil temperature through the generator was only 10-15 °C with an inlet

temperature of 150°C while air had a temperature increase of 75-85°C. This is due to the specific

heat of oil being twice that of air and because of the greater mass flow rate available for oil.

More recently, Schoning and Walti [5] introduced a comparison of the current generator cooling

4

techniques for high speed electric machines. The schemes are rated by the current density with an operating winding temperature of 250°C. Table 1 lists the current cooling systems with their maximum current density as well as the advantage and disadvantages of each system.

Table 1- Selected techniques for enhancing heat dissipation in high speed electric machines [5]

Cooling system	Current density A/mm2	Advantages	Disadvantages
Fins and heat sinks	5 to 8	Simple method	Increase in weight and size
Water or oil jacket	10 to 15	Effective stator cooling	Increase in diameter and weight
Direct liquid cooling and hollow conductors	up to 30	Very intensive cooling of the stator winding	Increase in weight and size Too expensive for machines rated below 200 kW
Spray oil-cooled end turns of rotor winding	over 28	Very intensive cooling of the rotor winding	Wet rotor; contamination of cooling medium (oil) with time
Liquid cooled wedges	8 to 15 (estimated)	Intensive cooling of rotor winding	Does not effectively cool the rotor poles
Cold plates between poles and rectangular wire rotor winding (IPS)	about 22 (estimated)	Intensive cooling of rotor winding	Requires installation of cold plates in rotor and cooling medium circulation

© 2011 IEEE

One design that is highlighted in the paper is a cooling system developed by Innovative Power Solutions (IPS). This 1 MW generator cooling design implements a new patent method for cooling the rotor poles and conductors. This method, shown in Figure 1, uses cold plates disposed between each rotor pole and field coil. While spray oil techniques reaches higher current densities than the cold plate design the plates have an internal cooling system that keeps the working fluid in a closed loop and out of contact with any electrical part.

5
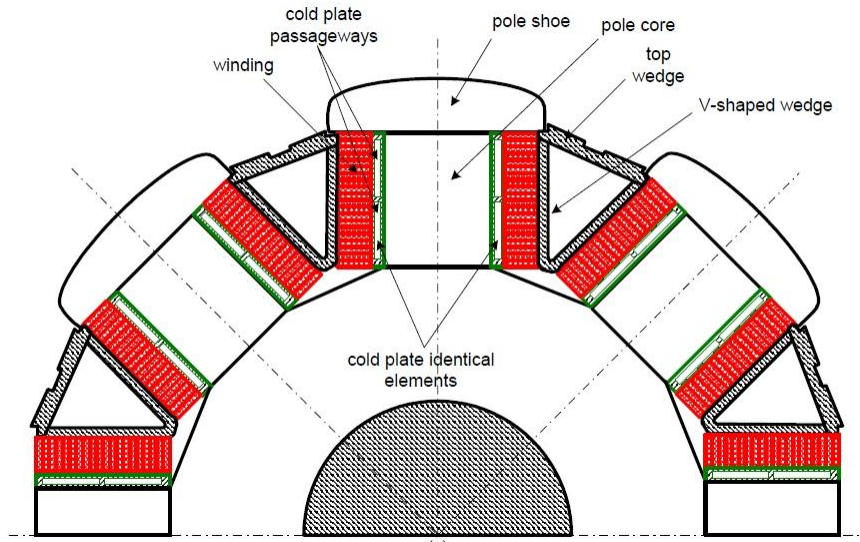
Figure 1- Construction of rotor poles and windings for cold plate design [5]

The cold plate design presented in U.S. Patent 6,661,133 [6] describes the fluid management and rotor assembly used for the cold plate design. This design, utilizing an internal parallel flow, is used as a baseline for comparing the three-layer impingement design used in this work. U.S. Patent 6,759,771 [7] also provides an internal parallel flow cooling scheme for an aircraft generator but instead of placing the cooling channels between the rotor pole and windings the cooling channel is placed inside the winding support wedges therefore utilizing a part of the generator already needed in the design. A detailed description of the fluid passage way from the rotor core to the rotor wedges is provided in the patent. While spray cooling, a hybrid of jet impingement, shows the most promise for cooling rotor windings the draw backs begin with the oil scavenging system and trying to maintain oil from entering the air gap between the rotor and stator. Windage loss occurs when oil fills into the air gap creating a drag force and

6

this loss increases greatly when the size and radius of the rotor increases. Many designs such as the cold plate patent have eliminated any possibility for oil to enter the air gap but have sacrificed the greater heat transfer coefficients spray cooling offers and therefore have increased weight or decreased electrical loads.

Free Jet Impingement

Martin [8] is one of the early and influential works on jet impingement for engineering purposes. It is a comprehensive survey emphasizing the engineering applications of heat and mass transfer between impinging jets and solid surfaces. Martin describes the flow pattern of impinging jets, seen in Figure 2, from single round and slot nozzles can be subdivided into three characteristic regions: the free jet region, the stagnation flow region, and the region of lateral (or radial) flow outside the stagnation zone, also called the wall jet region.
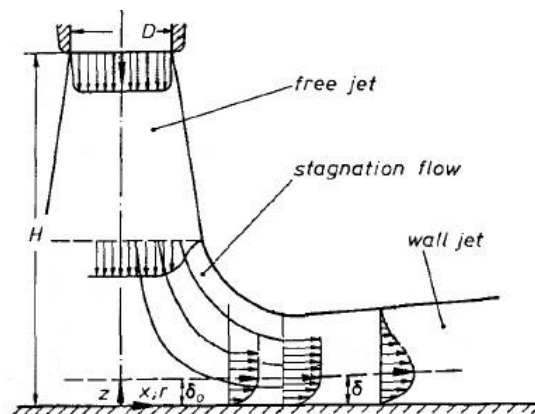
Figure 2- Flow field of impinging flow (schematically)

In a section titled "Heat and Mass Transfer: Variables and Boundary Conditions", Martin lists key hydrodynamic, thermal, and material boundary conditions that may be kept constant and must be considered. Two hydrodynamic boundary conditions are given by the distribution of velocities at the nozzle exit and the surface. It is presumed that all velocity components vanish at the surface and the fluid velocity at the nozzle exit is equally distributed over the cross section. The first assumption may never be met in practical applications but does not impose severe restrictions since the moving velocity of the material does not exceed a small fraction of the fluid impact velocity. The second assumption is fulfilled to a high degree of approximation since the exit jets are usually turbulent. A thermal boundary condition of importance is to presume the temperatures to be constant over the nozzle exit cross section. After determining local mass transfer coefficients and measuring local surface temperatures for both round and slot nozzles, the local variation in mass transfer coefficients shows a monotonically decreasing bell-shaped curve for large relative nozzle-to-plate distances H/d and curves with a more or less distant hump or second maximum for small H/d. Most influential of Martin's paper for this work was Chapter VII; "Optimal Spatial Arrangements of Nozzles". This chapter sought to find a combination of the geometric variables that yields the highest average transfer coefficient for a given blower rating per unit area of transfer surface. For uniformly spaced arrays of nozzles with good outlet flow conditions, there are always three independent geometric variables: nozzle diameter d, nozzle-to-nozzle spacing s, and nozzle-to-plate distance H. For jet Re between 2000 and 30,000 the optimal nozzle diameter is $d_{opt}=0.184H$, coinciding with the length of the potential core, and the optimal orthogonal array spacing is $s_{opt}=1.324H$. It is also noted that the transfer coefficients reached by the optimal round nozzle are about 8% higher than those for the optimal slot nozzle provided the blower rating, the pressure loss coefficients, and the nozzle-to-plate distances are

equal in both cases. Incropera et al. [9], in chapter 7, summarized key Nusselt number equations

listed in Martin for round and slot nozzles. These local and averaged Nusselt number equations

are given for different Prandtl number, Reynolds number, H/d, and nozzle exit cross-sectional

area to surface area cell A_r.

Confined and Submerged Jet Impingement

Pais et al. [10] was concerned with the possibility of flooding on the surface with the

coolant when miniaturization is imposed on nozzle sizes and nozzle-to-surface spacing. The flow

conditions are hence no more of a free jet impinging a surface but that of a submerged jet

configuration. The efforts of their study were geared towards single-phase heat transfer

characteristics of a submerged jet and to compare the performance with that of a free jet. The

liquid used in their study was a synthesized hydrocarbon fluid called PAO coolant (poly-alpha-

olefin) which had been developed by the Air Force for electrical and electronic cooling. The

experiments conducted had a circular jet nozzle of fixed diameter 0.76 mm with exit velocities

ranging between 5 to 15 m/s and jet-to-surface spacing ranging from 0.5 to 16 mm; 0.65 to 21

H/d. For all velocities tested Figure 3 shows that as the distance of the jet from the test surface is

increased the heat transfer at first increases, then decreases sharply reaching a minimum at

H/d~3. For any further increase of H/d the value of heat transfer coefficient increases steeply

and then levels out for H/d >11.
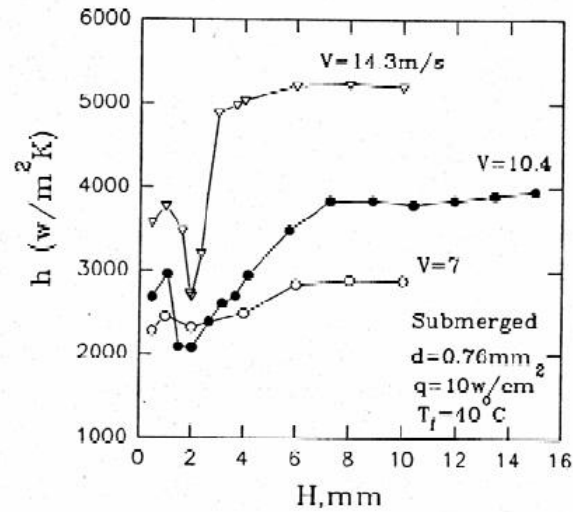
Figure 3- Effect of velocity V and the Distance H on the average heat transfer [10]

Figure 4 shows when the jet is submerged the temperatures on the surface can be as much as 33% higher than the free case and in all cases as the fluid flows away from the stagnation region the temperature of the surface raises rapidly. This is because 1) the liquid film velocity decreases as the fluid flows outwards, reducing the local convective heat-transfer coefficient and 2) the liquid is absorbing heat as its temperature rises and it flows outward.

10
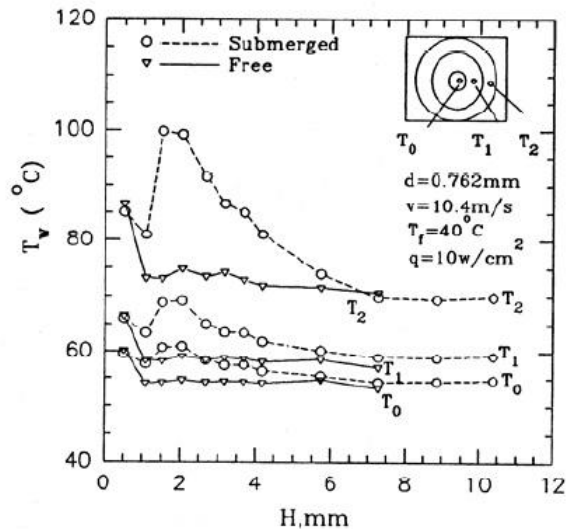
Figure 4- Surface temperature profile under the influence of free and submerged jets [10]

Chin-Yuan et al. [11] found that in spite of the large number of studies of jet impingement in literature a means for scaling the results, heat transfer coefficients and flow fields, between different fluids (with different thermo physical properties) and geometric parameters has not yet be developed for confined impingement. One of the main goals of the authors work was to develop predictive correlations for the stagnation and area-averaged Nusselt numbers in confined and submerged jet impingement, based on experimental results obtained over a wide range of fluid thermo physical properties. Single nozzle experiments using water with a range of parameters including Reynolds number, orifice-to-target spacing and orifice diameter were designed. Together with the experimental water jet results, results previously obtained for FC-77, and air similar techniques and facilities were used as a database to determine the effects of fluid properties (Prandtl number), and propose correlations that are valid for a

11

range of fluids. The author also sought out to no longer use a fixed exponent for Prandtl number, but instead, deduce this exponent based on an analysis of the experimental results. Table 2 presents Li's findings on area-averaged Nusselt-number correlations for a wide range of fluids.

Table 2- Area-averaged Nusselt-number correlations [11]

Fluid	Experimental parameters		Correlations[a]		Average (maximum) deviation (%)
Water	d	1.59–6.35 mm	$\overline{Nu} = 0.676\,Re^{0.555}Pr^{0.441}\left(\dfrac{\ell}{d}\right)^{-0.071}\left(\dfrac{D_e}{d}\right)^{-0.276}\cdot A_r$		3.52 (9.89)
	Pr	7.1–9.2			
	Re	8500–23000		(10)	
	H/d	1–4	$+1.113\,Re^{0.637}Pr^{0.441}\left(\dfrac{D_e}{d}\right)^{-1.062}\cdot(1-A_r)$		
	l/d	2			
	D_e	11.28 mm			
FC-77	d	1.59–6.35 mm	$\overline{Nu} = 1.347\,Re^{0.493}Pr^{0.441}\left(\dfrac{\ell}{d}\right)^{-0.071}\left(\dfrac{D_e}{d}\right)^{-0.276}\cdot A_r$		4.82 (15.77)
	Pr	20–25.2			
	Re	4000–23000		(11)	
	H/d	1–5	$+0.457\,Re^{0.736}Pr^{0.441}\left(\dfrac{D_e}{d}\right)^{-1.027}\cdot(1-A_r)$		
	l/d	0.25–12			
	D_e	11.28 mm			
Air[b]	d	3.18–12.7 mm	$\overline{Nu} = 1.828\,Re^{0.473}Pr^{0.441}\left(\dfrac{\ell}{d}\right)^{-0.071}\left(\dfrac{D_e}{d}\right)^{-0.312}\cdot A_r$		3.98 (13.19)
	Pr	0.7			
	Re	5000–23000		(12)	
	H/d	1–4	$+0.501\,Re^{0.724}Pr^{0.441}\left(\dfrac{D_e}{d}\right)^{-1.062}\cdot(1-A_r)$		
	l/d	1			
	D_e	22.56 mm			
Liquids	d	1.59–6.35 mm	$\overline{Nu} = 1.064\,Re^{0.513}Pr^{0.441}\left(\dfrac{\ell}{d}\right)^{-0.071}\left(\dfrac{D_e}{d}\right)^{-0.266}\cdot A_r$		8.03 (20.08)
	Pr	7.1–25.2			
	Re	4000–23000		(13)	
	H/d	1–5	$+1.291\,Re^{0.630}Pr^{0.441}\left(\dfrac{D_e}{d}\right)^{-1.063}\cdot(1-A_r)$		
	l/d	0.25–12			
	D_e	11.28 mm			
All fluids	d	1.59–12.7 mm	$\overline{Nu} = 1.179\,Re^{0.504}Pr^{0.441}\left(\dfrac{\ell}{d}\right)^{-0.071}\left(\dfrac{D_e}{d}\right)^{-0.283}\cdot A_r$		8.57 (27.79)
	Pr	0.7–25.2			
	Re	4000–23000		(14)	
	H/d	1–5	$+1.211\,Re^{0.637}Pr^{0.441}\left(\dfrac{D_e}{d}\right)^{-1.062}\cdot(1-A_r)$		
	l/d	0.25–12			
	D_e	11.28–22.56 mm			

Florschuetz et al. [12] provided an extensive look at flow distribution and heat transfer coefficients when two-dimensional arrays of jet orifice are required. Based on the cooling of the mid chord region of a gas turbine airfoil, the authors designed an experiment to determine the heat transfer behavior for a range of uniformly spaced array configurations. Figure 5 shows flow from the upstream span-wise jets in the array, y_n, imposing a cross-flow on those located downstream in the stream-wise direction, x_n.
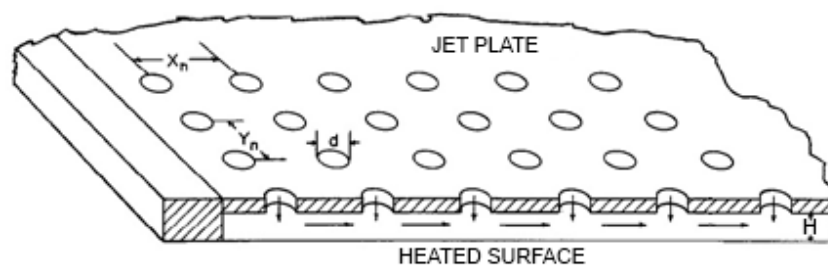
Figure 5- Basic test model geometry [12]

Correlations are presented for both inline and staggered hole patterns for Nusselt numbers resolved to one stream-wise hole spacing. Specifically, these Nusselt numbers are correlated in terms of the individual span-wise row jet Reynolds number, Re_j, and cross-flow-to-jet velocity ratio (G_c/G_j); and in terms of three geometric parameters: the stream-wise hole spacing, the span-wise hole spacing, and the channel height each normalized by the hole diameter(x_n/d, y_n/d, z/d). Two relevant conclusions are reached from this paper, one dealing with jet orifice flow characteristics the other on Nusselt number distributions along the stream-wise direction. The jet velocities for impingement with cross-flow are uniform when the parameter

13

$(y_n/d)*(z/d)$ is large. For the smallest value the distribution is highly non uniform with the jet velocity as small as one-half the mean at the first row, and as large as twice the mean at the tenth row. This can be seen in Figure 6. The local jet velocity-to-mean jet velocity is plotted for varying stream-wise hole spacing, span-wise hole spacing, and channel height.
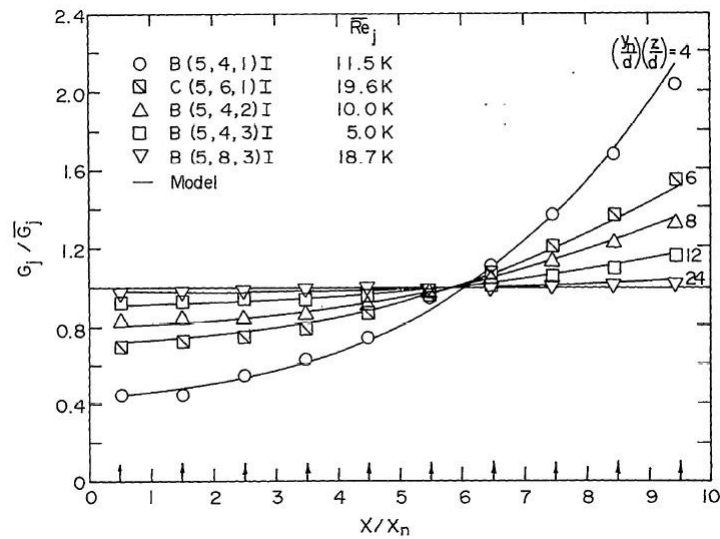
Figure 6- Stream-wise distribution of jet velocities
Comparison between measured values and model [12]

The experiments show that for all cases the local Nusselt number decreases along the stream-wise direction with the degree of decrease depending on the three geometric variables. The second relevant conclusion made deals with inline vs. staggered arrays when cross-flow is introduced. The tendency of the cross-flow to become channelized between adjacent stream-wise rows of the inline pattern reduces the direct influence it (cross-flow) can exert on each downstream jet. In contrast, the span-wise cross-flow distribution presumably remains more

nearly uniform for the staggered patterns. This effect is not significant for the largest hole spacing however as x_n/d and y_n/d decreases, and as z_n/d increases, the staggered pattern results in increasingly reduced heat transfer coefficients relative to the inline values for increasing cross-flow. Cross-flow effects are undesirable when the channel height-to-diameter is small, the span-wise distance is long. The flow distribution becomes non-uniform when $(y_n/d)*(z/d)$ is small.

Applications of Jet Impingement and the Use of Effusion Holes

Several types of cooling process have been introduced in the industry that have taken advantage of jet impingement and sought to effectively deal with cross-flow. One cooling system that has utilized jet impingement effectively is the Compact High Intensity Cooler (CHIC) [13]. The author sought a heat exchanger design that would involve both jet impingement heat transfer as well as thermal conduction. This was achieved by the use of impingement stacks. Effusion holes on the target surface were placed in a staggered array with the impingement holes to allow the fluid after impinging on the target surface to leave through the holes on the target surface. This process took place over a series of three to four stacks until the fluid reached the bottom target surface. After reaching the bottom surface the fluid leaves through channels located on the side of the structure until it reaches an outlet nozzle at the top of the model. The design configuration resulted in effective heat transfer coefficients based on the prime surface, of about 85,000 W/m^2 °C and 1.8 watts hydraulic power with liquid Freon 11 as coolant. The use of effusion holes to extract the impinging fluid locally has been studied when extraction is on the target plate as well as the impinging plate. Rhee et al. [14] studied jet impingement with local effusion holes located on the target plate. The author compared the heat

15

transfer characteristics of staggered effusion holes to shifted effusion holes. What was found

was that the secondary vortices are strengthened strongly and accelerated to the effusion holes

for the staggered hole arrangement, resulting in heat/mass transfer enhancement. Therefore, the

cooling of effusion plate with the staggered hole arrangement shows better performance than the

cooling with the shifted hole arrangement. Hoberg et al. [15] investigated effusion holes that

were located on the impingement plate instead of the target plate. The experiment tested an

impingement/effusion system that had a staggered pattern of jets, each surrounded by six evenly

spaced effusion holes. The experiment tested jet-to-target spacing between 0.44 and 4 and had

Reynolds number range from 500-10,000. Results showed that arrays with smaller diameter jets

were more effective at achieving the highest heat transfer coefficients and the larger heights

consistently led to lower heat transfer coefficients. Hoberg et al. [15] also compared his results

with correlations found in Martin [8] and Florschuetz et al. [12].

<u>Numerical Solutions for Impingement Cooling</u>

With the rise in computing power and the available CFD methods numerical solutions are

being used more often. Numerical solutions provide a cheaper method to estimate fluid flow and

heat transfer characteristics for many thermal models. Although jet impingement is a specific

case that many still believe can only be accurately predicted through experiments several sources

have used numerical solutions to confirm their experimental data. One of the most extensive

papers on jet impingement relevant to this topic is "Jet Impingement Heat Transfer" by

Zuckerman et al. [16]. This paper covers the physics, correlations, and numerical modeling

related to jet impingement. Zuckerman has collected many resources on jet impingement and

compiled all results and correlations. The paper covers topics such as flow regions, jet

geometries, cross flow and spacing effects, and experimental techniques for jet impingement.

While these are extensive one of the greatest contributions is its research on numerical modeling.

The author states that for jet impingement the difficulties in accurately predicting velocities and

transfer coefficients stem primarily from modeling of turbulence and the interaction of the

turbulent flow field with the wall. Steady and transient models are the two common categories

for turbulence modeling. The time-variant Large Eddy Simulation (LES) approach tracks flow

properties with the full equations down to some user defined length scale and then uses

additional sub-grid scale equations to describe turbulent flow behavior at smaller scales. The

LES method has shown encouraging results but requires high resolution in space for accuracy,

high resolution in time for stability and accuracy, and therefore needs a great amount of

computing power or time to produce satisfactory solutions for the transitional and turbulent

flows. Steady-state time averaged solution techniques, typically Reynolds-averaged Navier-

Stokes (RANS) models, use some version of the Navier-Stokes equations adjusted for the

presence of turbulent flow. As seen in Table 3 even with high resolution grids, the various

implementations of the k-ε, k-ω, RSM, and ASM models give large errors compared to the

experimental data sets. The v^2-f and SST models can produce better predictions of fluid

properties in impinging jet flows and are recommended as the best compromise between solution

speed and accuracy. In addition to the portions of the CFX model describing the fluid flow

inside the computational domain, the steady and transient models require a description of how

the flow behaves next to the wall or target surface. This part of the model typically plays the

major role in properly predicting both the flow and heat transfer. Numerical solutions have

shown that heat transfer rates within the viscous sublayer are a larger magnitude than outside the

17

layer. The special region in which the turbulence models have the greatest difficulty approximating the flow is the same region in which the largest heat and mass gradient occur, and so this region cannot be neglected. While some models have different ways to approach this near wall behavior the creation of computation cells near the wall is just as important.

Table 3- Comparison of CFD turbulence models used for impinging jet problems [16]

Turbulence model	Computational cost (time required)	Impinging jet transfer coefficient prediction	Ability to predict secondary peak
k–ε	★★★★ Low cost	★ Poor: Nu errors of 15–60%	★ Poor
k–ω	★★★★ Low–moderate	★★ Poor–fair: anticipate Nu errors of at least 10–30%	★★ Fair: may have incorrect location or magnitude
Realizable k–ε and other k–ε variations	★★★★ Low	★★ Poor–fair: expect Nu errors of at 15–30%	★★ Poor–fair: may have incorrect location or magnitude
Algebraic stress model	★★★★ Low	★★ Poor–fair: anticipate Nu errors of at least 10–30%	★ Poor
Reynolds stress model (full SMC)	★★ Moderate–high	★ Poor: anticipate Nu errors of 25–100%	★★ Fair: may have incorrect location or magnitude
Shear stress transport (SST), hybrid method	★★★ Low–moderate	★★★ Good: typical Nu_0 errors of 20–40%	★★ Fair
v^2f	★★★ Moderate	★★★★ Excellent: anticipate Nu errors of 2–30%	★★★★ Excellent
DNS/LES time-variant models	★ Extremely high (DNS available for low Re only)	★★★★ Good–excellent	★★★★ Good–excellent

[★ indicating undesirable model characteristics, to ★★★★ indicating excellent model characteristics.]

Kalitzin et al. [17] found that wall integration of turbulence models requires the first computational cell above the wall to be located within the viscous sublayer at about y^+=1. Kays [18] gives a detailed description of the critical value y^+. Experimentally we find that the sublayer thickness can be expressed in terms of y^+, and this value remains unchanged regardless of the total thickness of the boundary layer. The reason is that y^+ is simply a local thickness Reynolds number. Chougule et al. [19] and Tie [20] both conducted experiments that were comparable to numerical simulations they created. Chougule et al. [19] designed a simple round nozzle jet array of air impingement. The experiment had a range of Reynolds numbers from 7000 to 11,000 and a range of H/d from 6 to 8. These results were compared to an ANSYS ICEM CFD solution that utilized a shear stress transport (SST) turbulent model and comparable boundary conditions. The error in experiment to numerical calculations was no greater than 11%. Peng et al. [20] designed a liquid jet array experiment with comparable geometric parameters and Reynolds number to the present study. Fluent was used as the CFD modeler with a standard k- turbulence model. The experimental and numerical results fit well with a maximum uncertainty of 14%. Both papers show that correctly simulated numerical models have desirable results with small deviations from the experimental data.

CHAPTER 3 - METHODOLOGY

Overview

This work aims to provide an effective cooling method for high density electronic

devices. The process of research and design began with analyzing previous methods and patents

of cooling schemes. An effective method of cooling would take the benefits of the best heat

transfer methods while removing as many of the draw backs a theoretically and manufacturably

possible. One would not want to design a more thermally beneficial system only to create an

undesirable pressure requirement for the working fluid. A design utilizing jet impingement with

the inclusion of effusion holes was decided to be most beneficial. At this stage of development

the proposed technique needs to be tested for its ability to provide cooling. To find an optimal

design several key parameters in jet impingement need to be compared along with other

geometric parameters that would increase heat transfer coefficients. Once the range of variables

is decided a testing method is needed. While experimentation has been the tried and true way to

accurately test cooling designs, the increase in CFD modeling as well as the advancement in

computing power has allowed numerical simulations to gain similar footing for testing. With

this in mind, computer simulation software, ANSYS CFX, was used to predict the fluid and

thermal behavior of said design. Baseline models were also created, based off previous cooling

techniques listed in the literature, for comparison purposes. A brief look at the theoretical

equations and turbulence model used for simulating the flow field will be presented along with a

look at the geometry and boundary conditions of the design. It should be noted that much

research has already been done related to Reynolds and Nusselt number correlations for different

flow regimes of impingement. This work instead is focused on achieving an optimal cooling design under a given flow condition or mass flow rate.

<div align="center">Geometry</div>

The three-layer impingement design utilizes the heat transfer benefits of jet impingement while eliminating the negative heat transfer as a result of stream-wise flow for a long heated segment by utilizing effusion holes on the impingement plate. The major focus in design was to analyze a heated surface width of 24mm (1") and a surface length ranging from 24mm to 144mm (1" to 6"). The inlet and outlet ports were placed on the ends of the design with the fluid entering and exiting parallel to the heated surface, creating one flow direction. Figure 7 shows the flow of the cooling fluid moving within the first layer in the positive x (stream-wise) direction into the jet impingement nozzle. The impingement nozzles eject the fluid into the bottom layer. After impinging on the heated surface, the fluid is sent through the effusion holes located on the impingement plate into the middle layer where it then flows in the positive x direction towards the outlet.
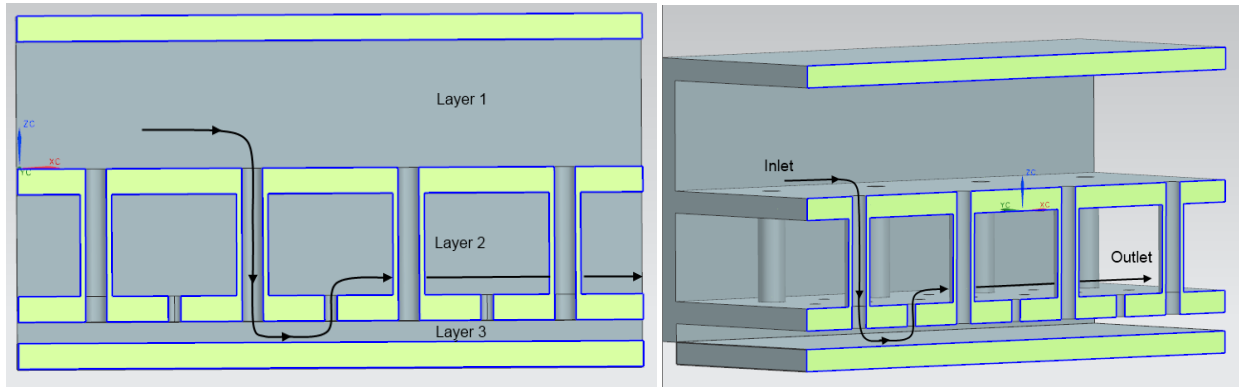
Figure 7- Three-layer flow pattern

The significant dimensions that would be unchanged throughout all the numerical tests were the jet impingement diameter (d = 0.838 mm) and the jet-to-jet spacing (s = 7.34d). Zuckerman [16] noted that for small scale turbomachinary applications, jet arrays commonly have jet diameter values of 0.2-2mm. The jet nozzles are placed in an inline configuration making the jet-to-jet spacing the same for the stream-wise and span-wise (y) direction. The height of both the inlet and outlet channels, first and second layer respectively, were specified to give uniform flow distribution across the entire length of heated segment, the inlet height for uniform jet impingement velocity and the outlet height for minimal pressure drop compared to the effusion holes pressure loss, and are therefore not dimensions vital to the heat transfer characteristics of the design. The jet diameter and jet-to-jet spacing were optimized for the mass flow rate used across all tested designs.

The first geometric parameter under analysis for its effects in heat transfer was the nozzle-to-impingement surface height (H). Common among literature is the non-dimensional variable, H/d, that sufficiently describes the jet to target height. This variable will be used for the rest of this paper. Three values of H/d are chosen that encompass the desired range for analysis;

23

six, three, and one. While some optimal values of H/d are discussed in literature for jet impingement, such as Martin [8], the case of submerged jet with the use of effusion holes is limited and therefore requires study to analyze H/d and effects in cooling.
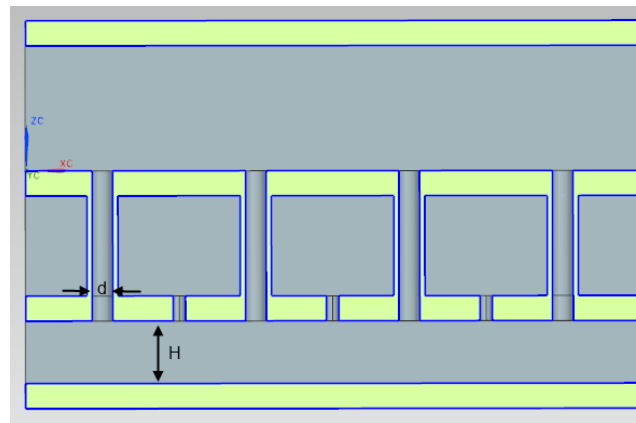
Figure 8- Three-layer design showing the jet diameter and jet-to-target height

The second geometric parameter that needed to be analyzed was the effusion orifice, specifically the diameter (d_{eff}) and arrangement. Since the design calls for a completely internal flow system, effusion holes on the target surface are inadequate. This lead to the placement of effusion holes on the jet impingement plate. Figure 9 shows the two arrangements that were used for the effusion hole design. The first arrangement was used only for the 0.5mm (small) effusion orifices. This arrangement, shown on the left, added effusion orifices in-line with the impingement jets as well as the staggered positions totaling 33 holes in the 1"x1" design. The second arrangement was used for the 0.838mm (medium) and 2mm (large) diameter effusion orifice and is presented on the right. The holes are equidistance from each other, 7.34d, and have been staggered with the jet orifices totaling 9 holes. The first arrangement provided more holes

on the surface of the plate in areas that jet interactions were known to occur while the second arrangement,0.838mm and 2mm effusion holes, would only be located at the areas that were known to have the least amount of impingement activity.
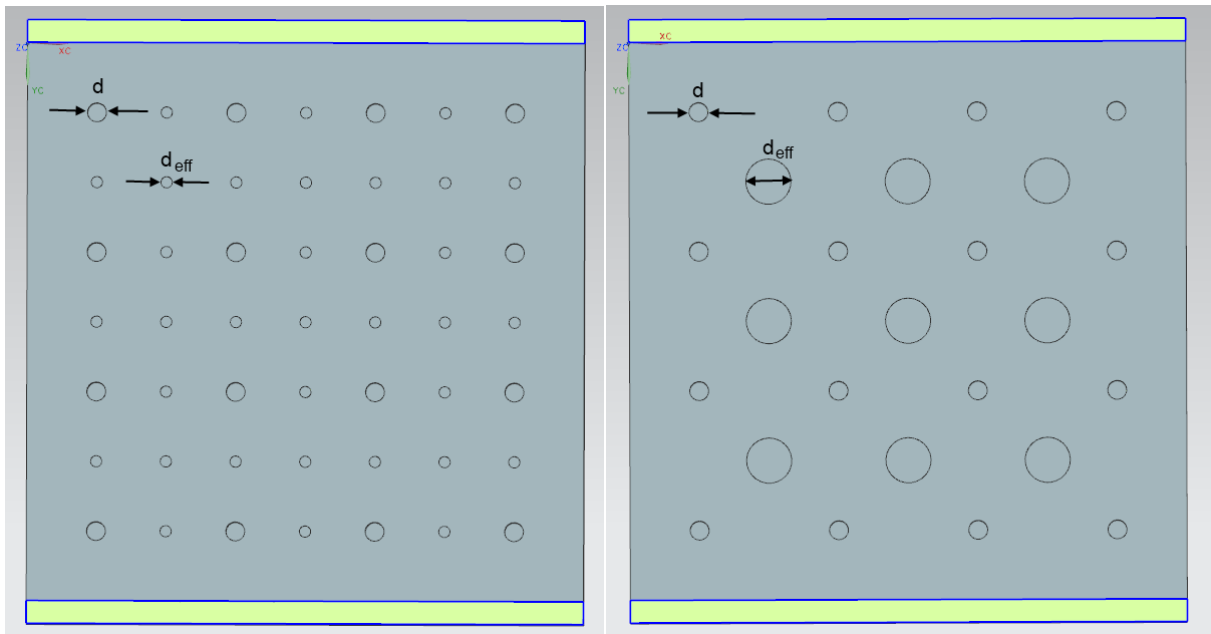
Figure 9- Jet impingement plate showing the jet diameters and effusion diameters

The final geometric parameter that would be analyzed for its heat transfer effects would be the addition of ribs on the heated surface. As stated by Zuckerman [16] the inclusion of ribs on the target or heated surface disturbs the wall jet, increasing turbulence as well as functioning as fins to increase the effective surface area for energy transfer. While many applications of ribs, also known as turbulators, include enhancing downstream turbulence such as a turbine blade, the ribs will most likely enhance heat transfer in this cooling system by acting as fins and directing the fluid to the effusion orifices located on the impingement plate. The ribs outline the area of

impingement for each jet nozzle and have a rib height-to-channel height ratio of 0.4. Figure 10 shows the arrangement of the ribs on the target surface. The ribs are separated from the walls of the model for the purpose of easy manufacturing. After analysis, conclusions might be found to show if the ribs would want to be extended to the edges to maximize heat transfer.
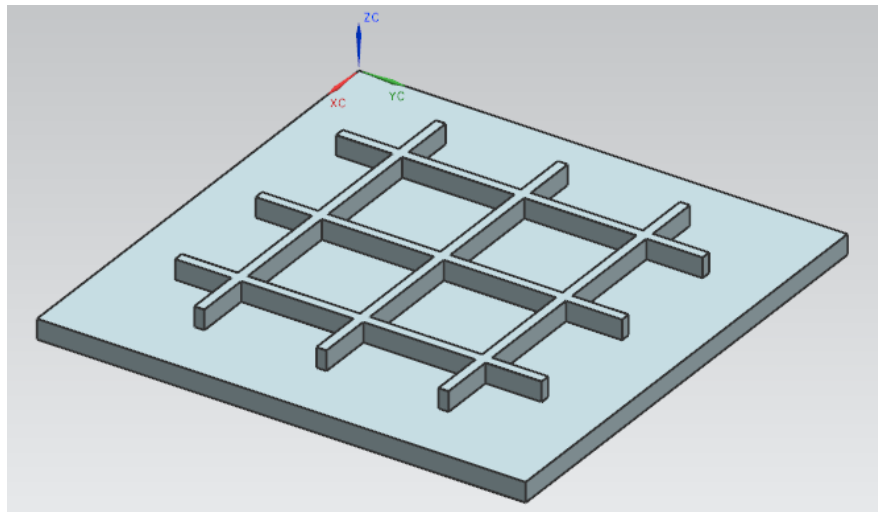
Figure 10- Small (1"x1") target surface with ribs

Governing Equations and Numerical Procedure

Multiple equations govern the physics behind the heat transfer involved in the three-layer design. The three laws required to solve the system, temperature and velocity, are the conservation of mass, momentum, and energy. For a three dimensional analysis the Cartesian equations can become long so a symbolic expression is used to describe the processes involved in each equation. The conservation of mass is the first equation needed to be used for numerical solutions.

$$\frac{\partial \rho}{\partial t} + \boldsymbol{\nabla} \cdot (\rho \boldsymbol{V}) = 0 \tag{1}$$

If we analyze an infinitesimal volume or point mass, the rate of change of the internal mass with respect to time is the net mass flow rate on the volume in all three Cartesian directions.

The conservation of momentum is the next equation needed and is analogous of Newton's second law of motion that states change in momentum is proportional to the impulse impressed on a body. In fluid mechanics, the application of Newton's second law leads to Navier-Stokes' equation, which is a differential form of the momentum equation, much like the continuity equation is for the conservation of mass. The general Navier-Stokes equations is given as

$$\frac{\partial (\rho \boldsymbol{V})}{\partial t} + (\boldsymbol{V} \cdot \boldsymbol{\nabla}) \rho \boldsymbol{V} = -\boldsymbol{\nabla} \mathrm{p} + \boldsymbol{\nabla} \cdot \boldsymbol{\tau} + \rho \boldsymbol{F} \tag{2}$$

The left side of the equation contains the product of density and total acceleration of the fluid. This total acceleration is broken down into the local and convective acceleration. If the problem is steady state and incompressible such as our case, then the local acceleration becomes zero leaving the convective acceleration only. The right side of the equation contains all the surface and body forces that are acting on the fluid element. The first two terms are the pressure gradient and the viscous forces, both of which are stresses in the fluid. The third term includes all the body forces. In most cases this term accounts for gravity acting on the fluid.

The final equation used is the conservation of energy equation. Since the flow involves

fluid at low speeds, the total energy equation can be simplified to a thermal energy equation.

$$\frac{\partial(\rho h)}{\partial t} - \frac{\partial \rho}{\partial t} + (\boldsymbol{V} \cdot \boldsymbol{\nabla})\rho h = \boldsymbol{\nabla} \cdot (\lambda \boldsymbol{\nabla} \mathbf{T}) + \mathbf{V} \cdot \boldsymbol{\nabla}\mathrm{p} + \boldsymbol{\tau} : \boldsymbol{\nabla V} + S_E \tag{3}$$

The left side of the equation contains the unsteady flow term, unsteady density term, and

the rate of change of energy due to flow work, convection, respectively. The right side includes

the conduction across the element, the work done by pressure, viscous dissipation, and internal

energy generation, respectively. Both the pressure term and viscous term on the right side are

derived from work done by shearing. If the flow is steady than the first two terms on the left side

become zero.

After the general equations had been provided, modifications needed to be made to

account for the turbulence that is found in the flow. Jet impingement takes special notice because

of the different fluid regions that exist in an impinging jet. Not only does the core jet region need

to be well modeled but also the wall boundary layers. While the present research has low

turbulence exiting the jet nozzle, turbulence modeling for this simulation is important and needs

to be tailored to the flow. A Reynolds Averaged Navier-Stokes (RANS) equation is one

approach to solving these equations. This starts by substituting the velocity $\boldsymbol{V}$ into an average

component $\overline{\boldsymbol{V}}$ and a varying component $\boldsymbol{v}$.

$$V = \bar{V} + v \qquad\qquad (4)$$

The average component is given by

$$\bar{V} = \frac{1}{\Delta t} \int_t^{t+\Delta t} V \, dt \qquad\qquad (5)$$

The Reynolds average total energy equation becomes

$$\frac{\partial(\rho h_{tot})}{\partial t} - \frac{\partial \rho}{\partial t} + (V \cdot \nabla)\rho h_{tot} = \nabla \cdot \left(\lambda \nabla T - \rho \overline{v\,h}\right) + \nabla \cdot \left(V \cdot \left(\tau - \rho \overline{v \otimes v}\right)\right) + S_E \qquad (6)$$

The equation contains an additional turbulence flux term $\rho \, \overline{v\,h}$ and the $\nabla \cdot \left(V \cdot \left(\tau - \rho \, \overline{v \otimes v}\right)\right)$ term is the viscous work term for total energy. A modified version is used for the thermal energy equation. From here Zimmerman [16] provides an analysis of several models used to close the averaged equations by computing the Reynolds stresses and fluxes. Zimmerman states that Menter's Shear Stress Transport (SST) model is one of the most successful Hybrid model. The SST model combines the k-ω model near the wall and the k-ε model farther from the wall to utilize the strengths of each. Smooth transition between the two models is accomplished by use of a blending function based upon distance from the wall. Chougule [19] also stated that SST k-ω model worked the best among the available turbulence models from an impingement flow condition giving accurate temperature and velocity measurements. While RANS models are less

accurate than the LES models that take into account the unsteady nature impingement can produce, run time and simplicity make SST a favorable choice.

Assumptions and Boundary Conditions

While conducting the present research, several key assumptions were made that are vital to the setup of the simulations and affect the outcome of the results. The first major assumption was to have constant thermo-physical properties for the working fluid. Many of the properties such as density, viscosity, specific heat, and thermal conductivity are dependent upon the fluid temperature. When there is a large change in fluid temperature or a property has a strong dependence on temperature, the assumption of constant property may not be valid. To determine if the present research can use the assumption of constant property across the whole fluid path, simulations were made using thermo-physical properties at different conditions that covered the range of temperatures found in the cooling scheme. Poly alpha olephin (PAO), the working fluid, is a synthesized hydrocarbon used as a dielectric cooling fluid for aircraft avionic systems and was the working fluid for this research. The temperature at inlet, film temperature, and heated surface temperature were the three temperatures used to calculate the PAO fluid properties. Nusselt numbers were compared using the constant fluid properties at 100 °C, 116 °C, and 136 °C with 100 °C being the base for comparison. The max, min, and average Nusselt numbers were recorded for the three-layer, 24.62 x 24.62 mm heated surface with 2mm diameter effusion holes. When the thermal properties were calculated at 116 °C, film temperature, the percent increase in Nusselt number was 8.7%. When the thermal properties were calculated at

136 °C, surface temperature, the percent increase in Nusselt number was 12.8%. The properties evaluated at inlet condition were sufficient to provide conservative results.

It is important to find if thermal radiation can be neglected when analyzing the three-layer cooling scheme. For many heat transfer problems radiation is a minor contributor compared to conduction and convection. A simulation was developed that included radiation using the Monte Carlo method. When compared with one of the 24.62 x 24.62mm heated surface models that did not include radiation a percent difference less than one existed. It can be concluded that radiation does not play a significant role in this cooling scheme. The Stefan-Boltzmann law relates heat transfer in radiation to the total temperature to the fourth power. Low absolute temperature in the solid body and working fluid leads to a relatively low emissive power. Buoyancy effects were also neglected due to the small change in density that exists in the working fluid making is safe to assume incompressibility. While some applications may have this cooling scheme submitted to rotational forces, such as an aircraft generator, the current model has no external forces applied to it. It is also assumed that the fluid is in a steady state condition. While turbulence has transient properties the RANS numerical method averages the transient properties or fluxuations, and forces the turbulent components into an averaged state. With low flow velocities the energy equation can be reduced from total enthalpy or total energy to a thermal energy equation by removing the kinetic energy terms from the energy equation.

Two domains are used within the CFX simulations. The fluid domain contains the fluid paths of the three-layer design including the inlet, outlet, impingement, and effusion channels. A 1mm thick, aluminum solid domain is located at the impingement surface of the fluid domain. A

conservative interface flux connects the two domains. Boundary conditions were placed at all external surfaces.
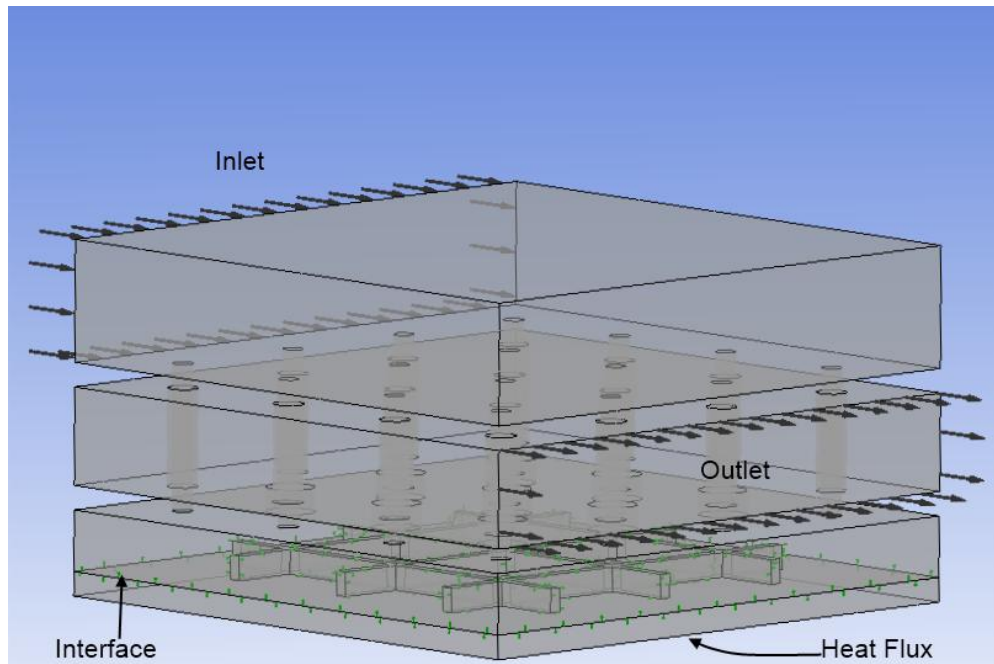
Figure 11- Boundary conditions for the small three-layer model

An inlet condition was placed at the entrance to the 1st layer with a specified flow condition and temperature. For the small model, 24.62x24.62mm heated surface, a mass flow rate of 0.0365504 kg/s was assigned with a subsonic, turbulence intensity of 1% and a static temperature of 100 °C. The mass flow rate provides an average Reynolds number across the jet nozzles to be 2800. When the geometry changes for models with elongated heat flux surface the mass flow increases to keep the average Reynolds number of the jet nozzles at 2800. The outlet condition was placed at the exit of the 2nd layer. An area average static pressure of zero was used. In the solid domain, a heat flux of 23 W/cm^2 was imposed on the bottom surface. This

heat flux was comparable to a heat source given in an aircraft generator. All other surfaces were specified with a smooth, no slip, and adiabatic wall condition.

Mesh Setup

When solving the governing equations that are used to find the temperatures and velocities of the system, simulations require a number of smaller cells or elements that make up the whole system. The collect of all these elements is called a grid or mesh. Within each of these cells, the governing equations are discretized and solved iteratively. When the solutions are collected and put together, a detailed description of the fluid and or solid can be found for the entire system. The more cells that are incorporated the more accurate your solution becomes. There are limits to how beneficial addition elements becomes and this is based on the convergence of the simulation. Ideally the researcher aims to have a mesh independent solution, meaning the addition of more elements does not benefit the model and the model has converged completely. Residuals are set up to determine the amount of error tolerable from the true value and if the solution is converging the solver will stop when an iteration has reached a solution within the residual. The importance of mesh size and the number of elements is to guarantee the converged solution is the correct solution. If the mesh is too coarse the numerical solver could produce inaccurate results. ANSYS CFX has automatic mesh generator based on specifications by the user as well as the intended solver being used for simulation. Since the mesh used in this research was based off CFX's automatic made mesh, the important changes will be presented.

Tetrahedral elements were the main elements used in the fluid and solid domain. A patch-conforming mesh method was chosen which creates the surface mesh first, then the

volume mesh. This mesh choice provides the ability to add mesh controls later on to improve the

accuracy in critical areas, such as the impingement surface. The relevance or fineness of the

mesh was set to Fine and the smoothing was set to High. In total, most of the 18 simulations

used to compare the three-layer model had over one million elements in the fluid domain. The

surface meshing was set to Curvature and Proximity which allows for a refined mesh around

curves and edges as well as a set number of cells across a narrow gap. This becomes important

for the case of ribs on the impingement surface. Default values were used for the number of

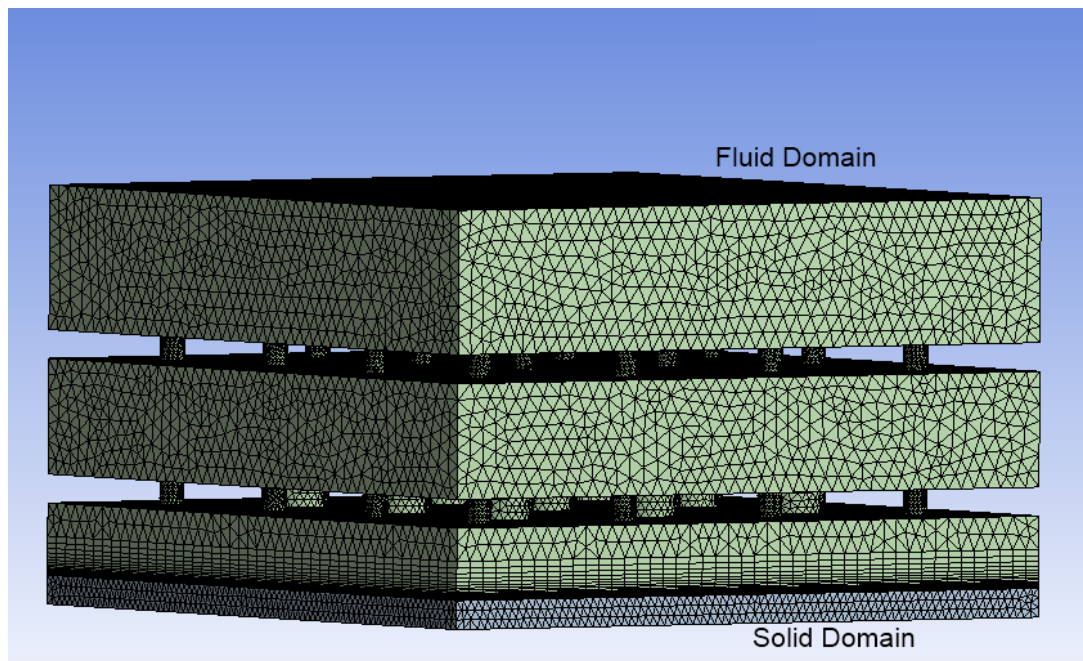cells and span angle, 3 and 18 respectively.

Figure 12- Mesh for three-layer design including the solid and fluid domain

A key control added to the mesh was the addition of inflation layers on the impingement

surface of the fluid domain. Inflation layers are added to a surface when the cell height needs to

be refined within a certain distance. The inflation layers are generated based on three key parameters. The first is First Cell Height. For this model the first cell height was intended to have a y+ less than 1. To achieve this, a height of $5\text{x}10^{-6}$ meters was used for H/d of 3 and a height of $2.5\ \text{x}10^{-6}$ meters for H/d of 1 and 2. The second critical parameter was height expansion ratio. This was set to 1.2. The final parameter was the number of inflation layers. This value depended on the bottom layer height. The goal was to have one or two unrefined cells in the bottom layer. For H/d of 1, 2, and 3 the number of inflation layers was set to 20, 24, and 22 respectively.
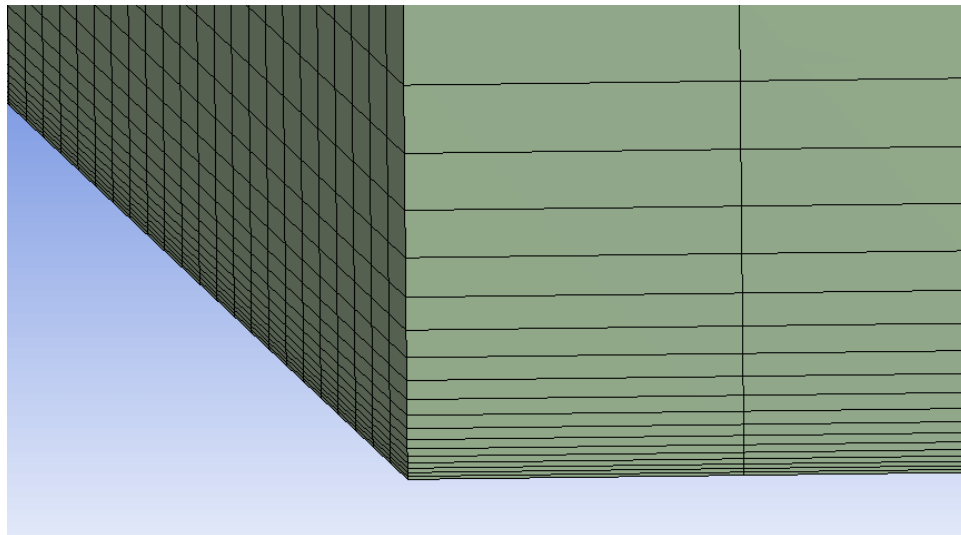
Figure 13- Inflation layers on the impingement surface

The first cell height was the critical meshing value and is agreed as the variable that determines if the model is grid independent. To find out if the first cell height was adequate, we test varying cell heights. The tested cell heights were $5\text{x}10^{-7}$ m, $5\text{x}10^{-6}$ m, $5\text{x}10^{-5}$ m, and a model with no first cell height given for a H/d=3 model with 2mm effusion holes and a heated surface

with ribs. Figure 14 shows the average Nusselt number for each height configuration normalized to the finest mesh simulated.

First Cell Height for H/d=3, 2mm deff, with ribs

Figure 14- Temperature distribution and Nusselt number comparison for varying meshes

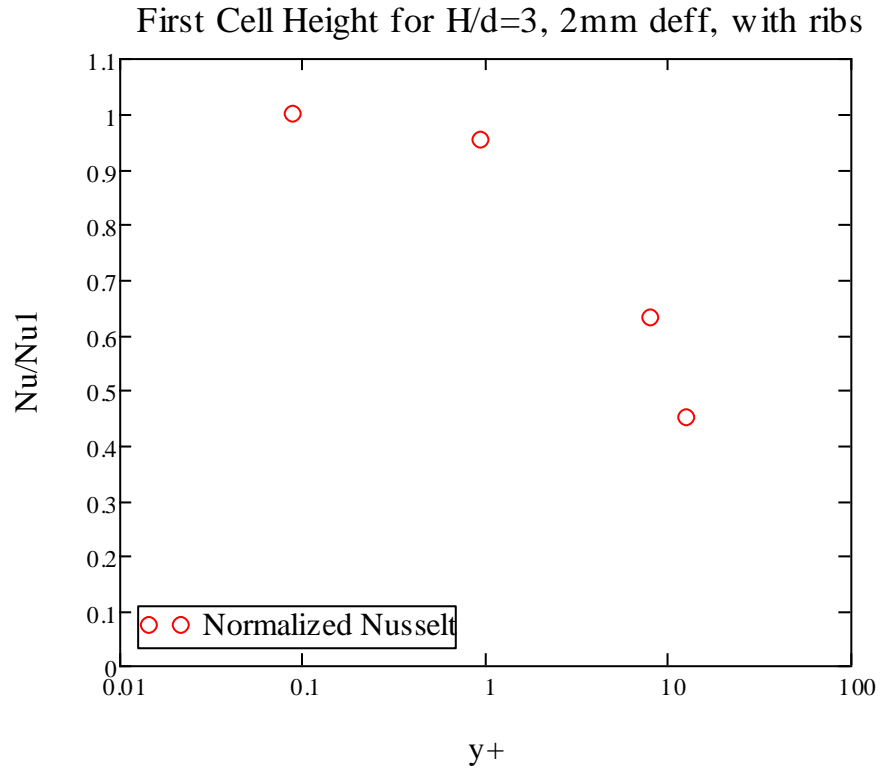It can be seen that once the cell height was within the y+ value of 1 a decrease in first cell height provided minimal improvement in Nusselt number. It was assumed that providing a first cell height less than y+=1 was sufficient to provide a mesh independent model in the z direction.

Nusselt Number Correlations

Much research is spent examining heat transfer coefficients for jet impingement. The basic convection heat transfer equation, Newton's law of cooling, is expressed in the form

$$q'' = h(T_s - T_{in}) \tag{7}$$

Where

$$Nu \equiv \frac{h d_h}{k} \tag{8}$$

For most jet impingement cases, the heat transfer coefficient over a given surface area is desired making the average Nusselt number the main focus for data collection. This is obtained by integrating the local results over the given surface area. Incorpera [9] states for a free jet that the average Nusselt number, a dimensionless quantity, is a function of

$$\overline{Nu} = f(Re, Pr, A_r, H/d_h) \tag{9}$$

Where

$$A_r = \pi d^2 / 4s^2 \tag{10}$$

This shows that the three main geometrical parameters for finding the heat transfer

coefficients are jet-to-target spacing, nozzle diameter, and jet-to-jet spacing while the fluid

identities required for calculation are the Reynolds number and Prandtl number. Martin [8] gave

the correlation for round nozzle arrays with the range of validity: 2,000< Re<100,000;

0.004≤A$_r$≤0.04; 2000≤H/D≤12.

$$\overline{Nu} = Pr^{0.42}(K)(G)(F) \tag{11}$$

Where

$$K = \left(1 + \left(\frac{H/d}{0.6/\sqrt{A_r}}\right)^6\right)^{-0.05} \tag{12}$$

$$G = 2\sqrt{A_r}\frac{1 - 2.2\sqrt{A_r}}{1 + 0.2\left(\left(\frac{H}{d}\right) - 6\right)\sqrt{A_r}} \tag{13}$$

$$F = 0.5Re^{2/3} \tag{14}$$

When geometric boundaries, such as top and side surfaces, constrain the fluid flow paths

the heat transfer characteristics are no longer defined by the correlations above. In most cases,

the heat transfer coefficients decrease, particularly when the spent jet fluid interacts with other

jets developing a cross-flow in the stream-wise direction. Florschuetz [12] deduced that the

Nusselt number is now affected by the ratio of cross-flow mass velocity –to-jet mass velocity.

Since Florschuetz was testing within the range of parameters used for this research the

correlations used for confined flow will be of importance, specifically for validating the results

of this research, and therefore these Nusselt number correlations will be presented in detail.

Florschuetz adapted the following form

$$Nu = A\,Re^m\{1 - B[(H/d)(G_c/G_j)]^n\}Pr^{1/3} \tag{15}$$

The coefficients A and B, and the exponents m and n are each permitted to depend on the geometric parameters in the form of simple power functions.

$$A, m, B, n = C(x_n/d)^{n_x}(y_n/d)^{n_y}(H/d)^{n_H} \tag{16}$$

Table 4- Constants for Use in Correlation Equation [12]

	C	n_x	n_y	n_H
Inline Pattern				
A	1.18	-0.944	-0.642	0.169
m	0.612	0.059	0.032	-0.002
B	0.437	-0.095	-0.219	0.275
n	0.092	-0.005	0.599	1.04

For the sake of this research $x_n/d \equiv y_n/d \equiv$ s. This correlation does not account for effusion orifices or ribs on the heated surface. The research done by Florschuetz only included H/d for 1,2 and 3. Figure 15 shows the average Nusselt number plotted for a stream-wise jet distance. In the graph below, x_n represents the stream-wise row of jet orifices. In this case the cooling scheme has 12 stream-wise rows of jets. The correlation plots show the effect cross-flow

has on the average Nusselt number for each stream-wise row. The graph includes two plots, one

for H/d of 2 and the other H/d of 3.
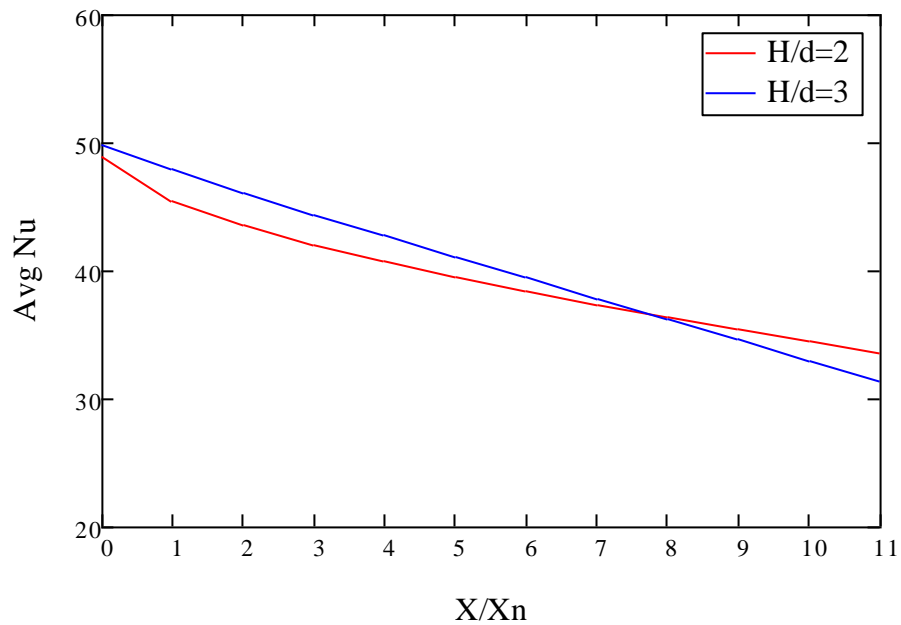
Figure 15- Stream-wise distribution of average Nusselt number

The cross-flow functional form would have to be monotonically decreasing for most

values of x_n/d, y_n/d, and H/d but for some cases, with $H/d = 1$,would have to allow a broad

shallow minimum. From the chart we can see that cross-flow for long stream-wise distances

decrease the local and average Nusselt number over the heated surface. The goal of the present

research is reducing this decline in heat transfer coefficient.

CHAPTER 4 - RESULTS AND DISCUSSION

The process of collecting data and developing correlations during this research was continuous and frequently evolving. When developing new techniques for cooling, finding the right variables that are significant enough to be analyzed is many times the most important step, one that seems to never be completely solved. When one question was answered two more were presented. The results found during testing were significant and difficult to narrow down. However, the present work revealed key aspects and trends of the three-layer cooling design that will indeed provide the means of creating an optimal cooling scheme.

To find the optimal design, combinations of three goals were set. The first was to obtain the highest heat transfer coefficients available for a given mass flow. To quantify this goal an area-averaged heat transfer coefficient was found on the heated surface. While this does not represent the temperature field of each model it provides the best solution for finding an overall difference in each model. Plots of each heated surface will be compared and analyzed to provide a more detailed look at each models cooling process. The second goal was to find the configuration that provided the heated surface with the most uniform temperature distribution. For the sake of this research $\frac{dT}{dx}$ is not what will be looked at but the overall temperature difference on the surface ΔT. The third goal was to find a design that maintained a reasonable amount of pressure drop for the given heat transfer coefficient. As mentioned before, it wouldn't be beneficial to have a high heat transfer coefficient but an unreasonably high pressure drop in the system. Another goal that is desired from this research, but not primary, is to find a well defined trend among the variables used in this research so that the optimal design could be

tailored to a specific factor that may be needed in further research or design. Like the research preceding it, dimensionless and normalized values will be used when possible to describe the results of the simulations. A total of 18 simulations were used to compare the variables used in this research, each containing a 24.62 x 24.62mm (1"x1") heated surface.

<div align="center">Average Heat Transfer Coefficients</div>

The average heat transfer coefficient shows the overall effectiveness of the cooling scheme. Equation 7 and Equation 8 provide the formulas for determining the heat transfer coefficient. The input parameters of the simulation are the heat flux on the surface per unit area and the inlet fluid temperature. The simulation provides the surface temperature needed to solve the rest of the equation. It should be noted that within the Post-Processing of simulation, two different options are provided when finding a value on a surface element such as the heated surface. Within CFX, hybrid and conservative values can be given for most variables. Conservative values are used most often except at specified boundaries such as a no slip condition or a heat flux condition. Simply put, conservative values are the element average value while the hybrid values are given at the specified boundary. For our purpose hybrid values are used since the temperature at the heated surface is what we are looking for. More specifically, since this cooling design is meant to be in contact with another object that provides the heat source, surface temperatures on the bottom of solid body will be used for the heat transfer equations. Figure 16 shows the average Nusselt number plotted for each of the 18 simulations.
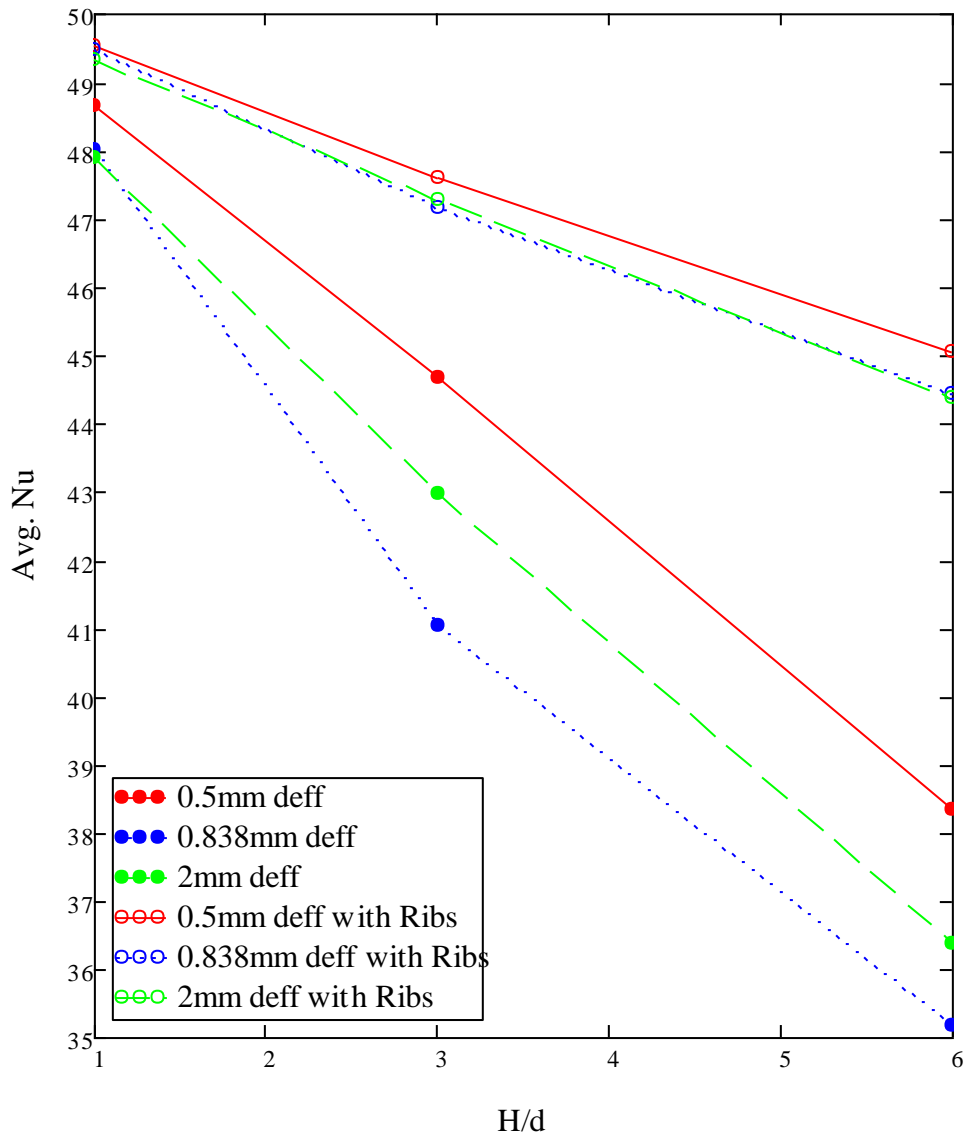
Figure 16- Effects of H/d on the average Nusselt number

Of the three variables under analysis, the heat transfer coefficient appears to have the strongest dependence on H/d. A linear decrease occurs as H/d becomes larger. Table 5 shows the heat transfer coefficients normalized to the maximum average reached during simulation, the coefficient given at H/d=1.

Table 5- Effects of H/d on heat transfer coefficient

Normalized Heat Transfer Coefficient to H/d=1

	w/out Ribs			w/ Ribs		
H/d	0.5 mm d_{eff}	0.838mm d_{eff}	2mm d_{eff}	0.5 mm d_{eff}	0.838mm d_{eff}	2mm d_{eff}
1	1.00	1.00	1.00	1.00	1.00	1.00
3	0.92	0.85	0.90	0.96	0.95	0.96
6	0.79	0.73	0.76	0.91	0.90	0.90

Since the maximum heat transfer coefficient is our goal, this value will be our point for comparison. When the cooling system does not have ribs on the heated surface the heat transfer coefficient is 10-15%% less at H/d =3. At H/d=6 the heat transfer coefficient ranges from 24-29%. less. When the cooling system includes ribs on the heated surface the heat transfer coefficient does not reduce at the same rate as a design without ribs. The coefficient only decreases 4-5% for H/d=3 and 9-10% for H/d=6.

The second strongest parameter affecting the average heat transfer coefficient was the addition of ribs on the heated surface.

Table 6- Effects of ribs on the heat transfer coefficient

Analysis with Ribs

`	Percentage Increase with Ribs		
H/d	0.5 mm d_{eff}	0.838mm d_{eff}	2mm d_{eff}
1	1.8	3.1	3.0
3	6.6	14.9	10.0
6	17.6	26.3	21.9

From Table 6 we can see that the addition of ribs affects the heat transfer coefficient differently for each H/d but always with an increase in transfer coefficient. For small H/d, the addition of ribs is minimal, 1-3% for H/d=1. When H/d=3 the ribs have a 6-15% increase and for H/d=6 there is a 17-26% increase. The increase in heat transfer can be due to the length of fin as well as the ribs directing the fluid towards the effusion holes.

The effusion hole diameter and arrangement are the parameters that have the least amount of impact on the average heat transfer coefficient. The effusion diameter and arrangement does not directly impact the jet impingement process, but one might be able to make an assessment concerning the arrangement of effusion holes from the results. It can be seen in Figure 16 that the design containing the most amount of holes, 33 small holes placed on the effusion plate as compared to the 9 hole arrangement used for the medium and large diameter arrangements, provided the best heat transfer in every case. This might imply that the design with the larger amount of effusion holes provides the best evacuation of the spent fluid leading to a high heat transfer.

Temperature Distribution on the Heated Surface

After each of the 18 models had been simulated, a temperature plot was produced for each heated surface. Each plot shows an outline of the impingement holes, effusion holes, and ribs, according to each model.
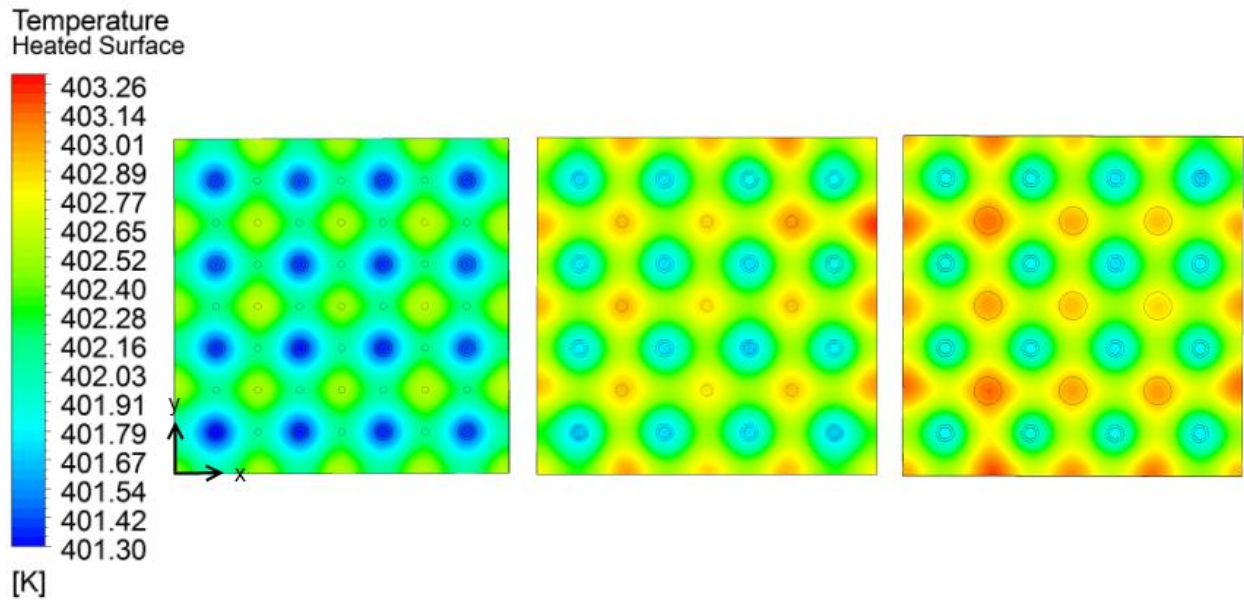
Figure 17- Effects of effusion holes on surface temperature for H/d=1

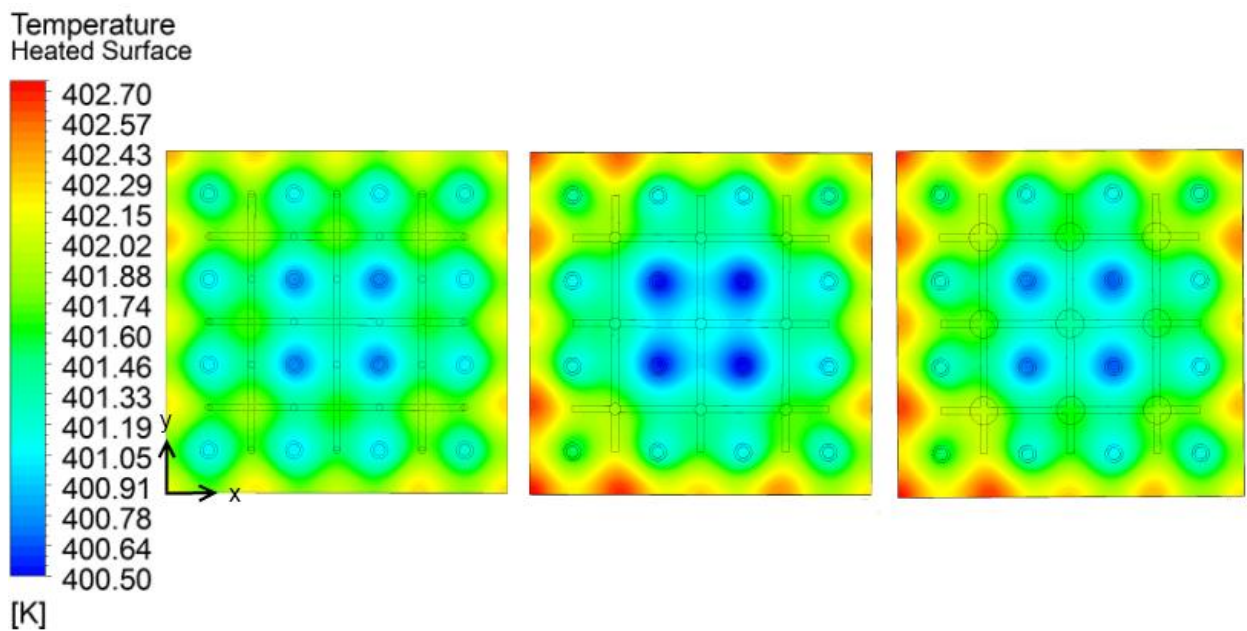

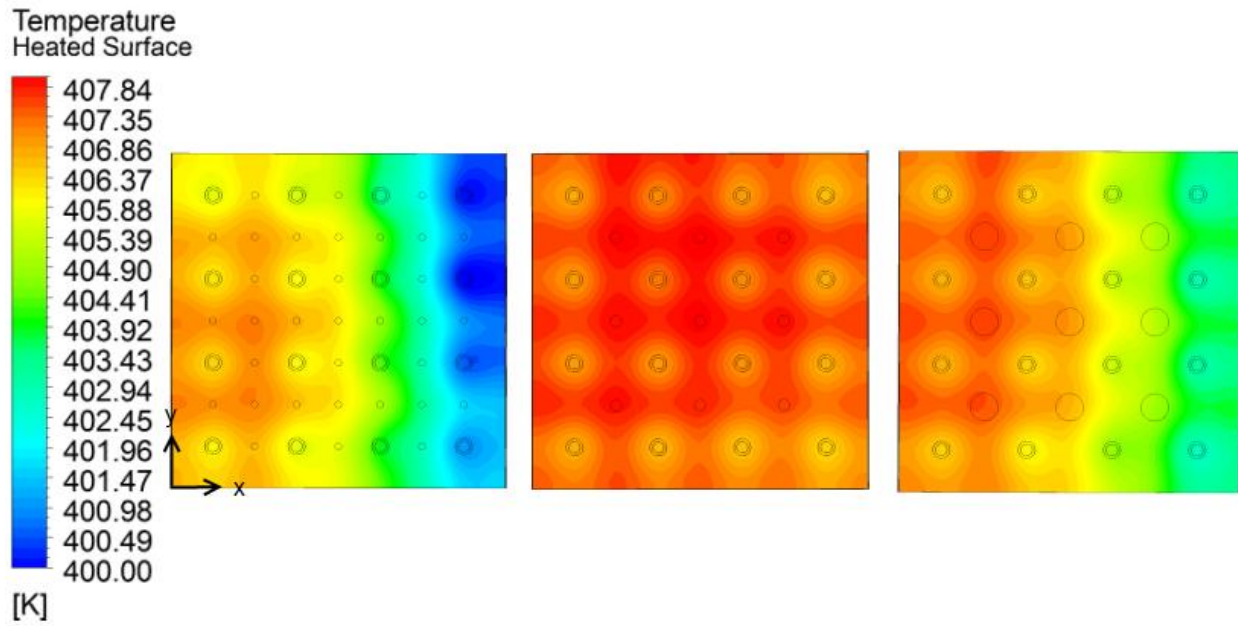Figure 18- Effects of effusion holes and ribs on surface temperature for H/d=1

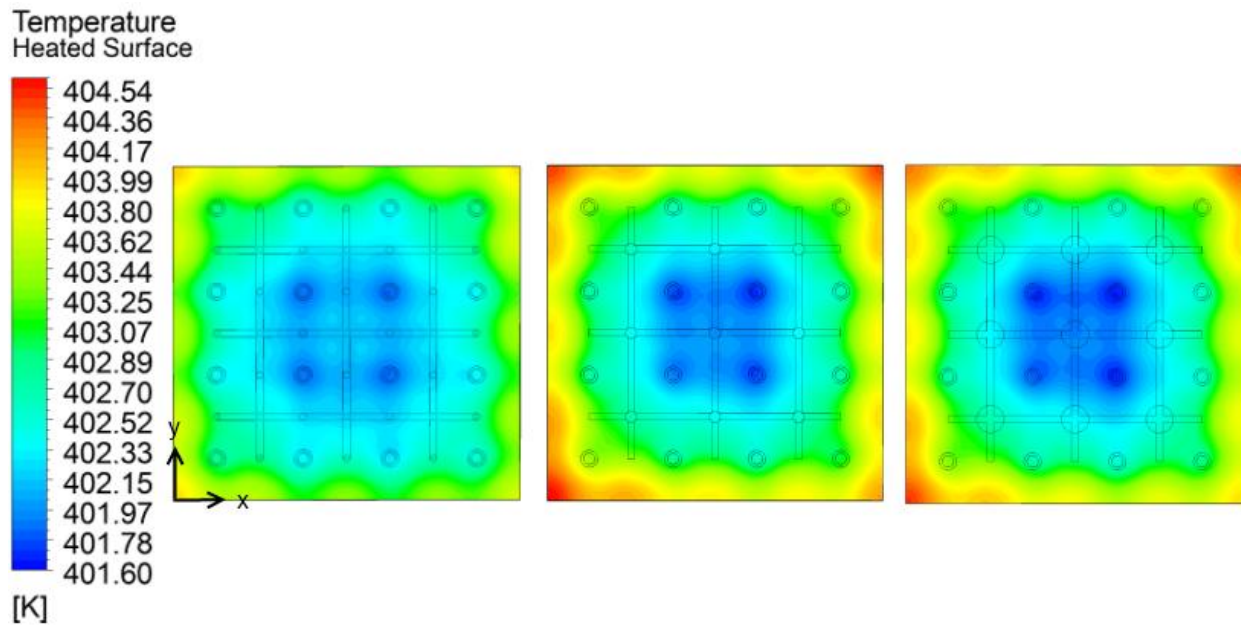Figure 19- Effects of effusion holes on surface temperature for H/d=3

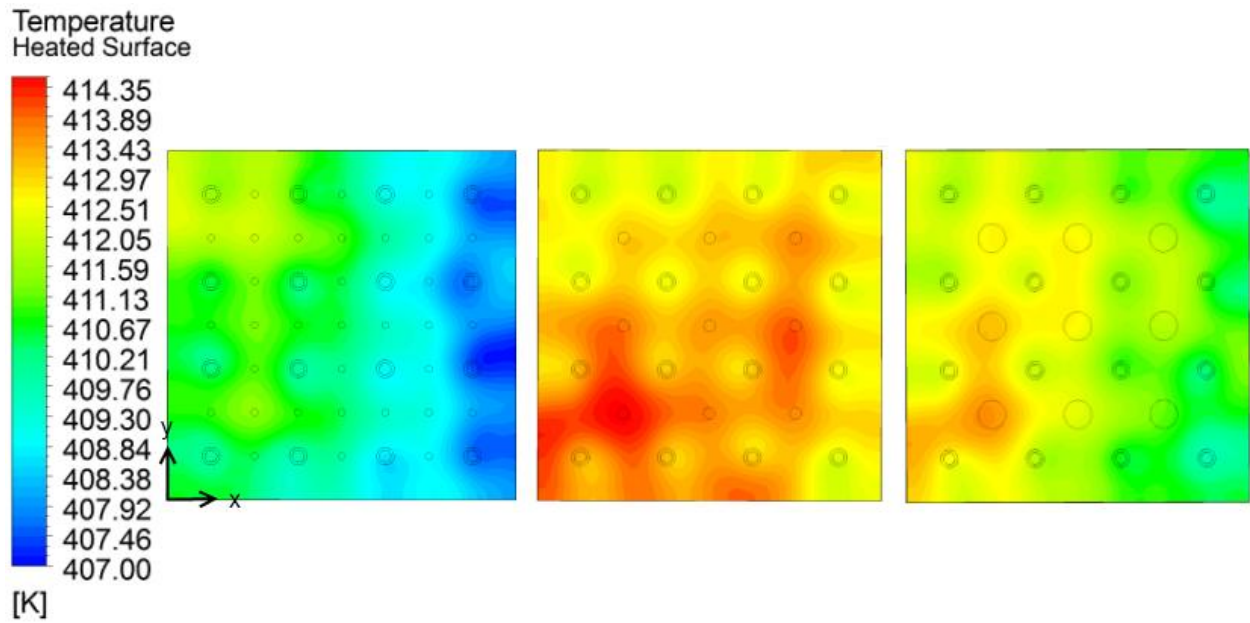Figure 20- Effects of effusion holes and ribs on surface temperature for H/d=3

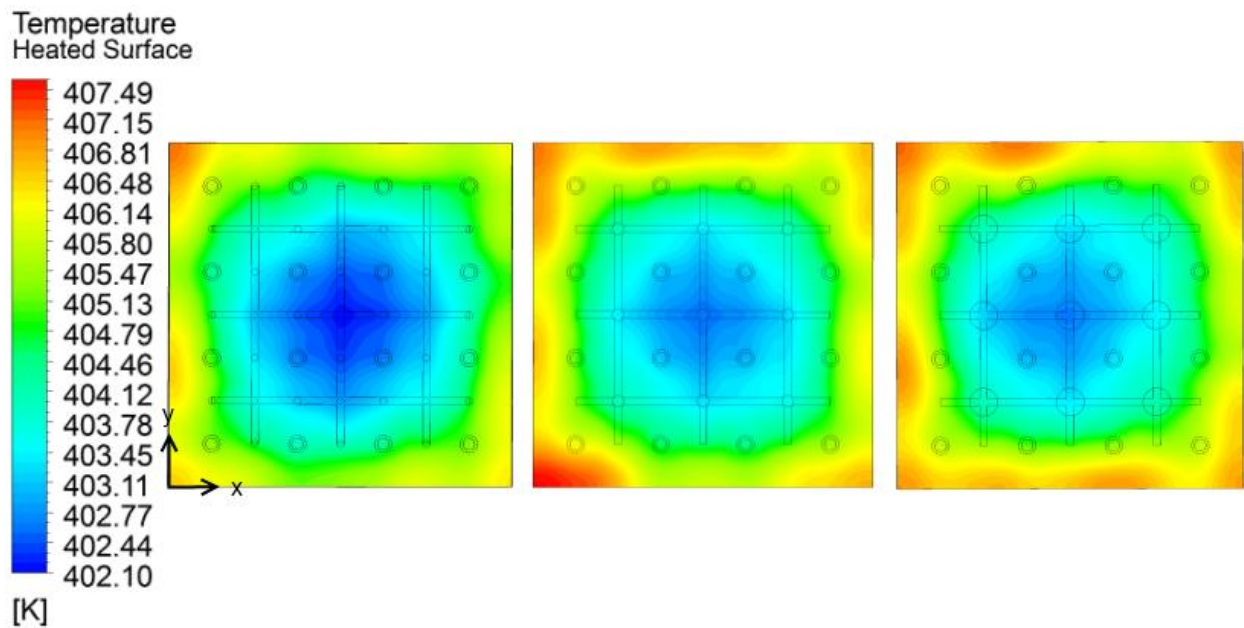Figure 21- Effects of effusion holes on surface temperature for H/d=6

Figure 22- Effects of effusion holes and ribs on surface temperature for H/d=6

The heated surface temperature plots provide a good representation of how the impinging fluid is interacting with the surface and how the surface is distributing the heat at the bottom. We will first look at the models having H/d=1. The temperature plots for non-ribbed surfaces shows a symmetric distribution of impingement from the stagnation point to the outer regions for each jet. The hottest points are located furthest away from the jets and are all the same temperature. The models that include ribs have cooler regions at the center but the temperature distribution from the stagnation region outwards, for each jet, is still well defined. The hottest points are located at the outer edges of the heated surface.

When H/d=3 the temperature plots become less symmetric. The jet stagnation regions are still recognized but the location of impingement is not directly below the jet nozzles. There are varying hot spots indicating a small amount of mixing within the chamber. For models that include ribs, the coolest spots are located at the center of the surface. The impingement regions are less noticeable than for H/d=1, but like H/d=1 the hottest spots are located at the outer edges of the surface are fairly distributed around the edge.

When H/d=6 the temperature plot is not symmetric in the x or y direction of the surface and trends are harder to recognize. When the heated surface does not have ribs the impingement regions vary in cooling intensity and are not always located below the nozzles, much like the case for H/d=3, and impingement regions are hard to distinguish. When ribs are included on the heated surface the impingement regions are not recognizable. The ribs have centralized the cooling areas. If a temperature plot was given at the interface of the fluid and solid domain, the impingement regions would be more recognizable.

After analyzing the streamlines of a model with ribs verses a model without the fluid is indeed directed by the ribs. This of course becomes less dominate when H/d decrease. When H/d=1 the benefit of ribs is much smaller than that of H/d= 3 or 6. Figure 23 shows the temperature plot of the interface between the solid and fluid domain for H/d=3.
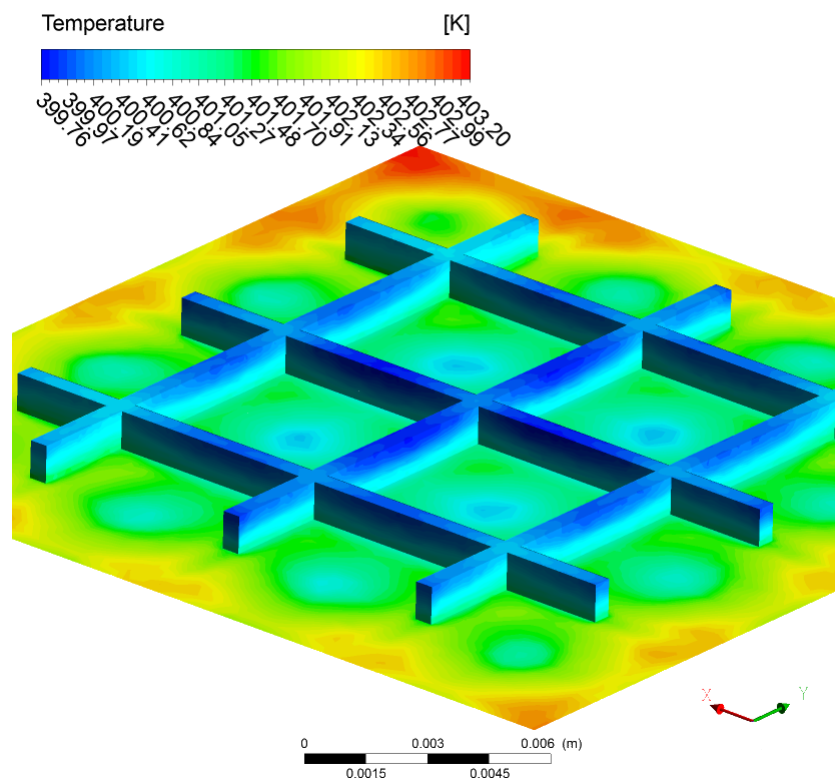

Figure 23- Temperature plot of the fluid-solid interface of the heated surface with ribs (1"x1")

While the thickness for each rib remains the same for all models, the height is dependent on H/d. The cooler impingement regions are in the center of the model but only are increased by less than 1°C for most cases. It can be seen that the ribs act as fins on the surface where

50

temperatures of less than 400 k are reached. The coolest parts of the ribs are in the thinnest

sections. When the ribs come together the thickness reduces the ability to transfer heat

effectively. Changes could be made in the future to develop a uniform thickness at the junction

points or variable thickness as the height increases. The decision to not have the ribs extend to

the edges of the heated surface was for easy manufacturing but this could also be changed. If the

ribs were extended to the edges heat transfer would increase at those spots and would not

centralize the cooling as much as the present model does. The hypothesis for better rib

performance at higher H/d is due to the height of each rib increasing. It is also believed that the

rib height creates uniformity in the impingement regions. The interaction of jets and spent fluid

in H/d=3 and H/d=6 is reduced when the ribs are introduced to the model.

Pressure Drop across the Model

The pressure drop across the three layer design consists of five main sections; the inlet

channel, impingement nozzle, impingement channel, effusion nozzle, and outlet channel. While

there is pressure drop that is calculated for each channel length and nozzle length, the nozzles for

impingement and effusion have minor losses as well. These losses occur at the sudden

contraction leading into the nozzle and the sudden expansion leading out of the nozzle. Of these

sections only one differs for each model enough to create a significant pressure difference, the

effusion nozzle. To look at the pressure drop across the effusion holes we will consider the loss

due to contraction and the loss across the nozzle length utilizing pressure loss equations from

Fox et al. [21]. Equation 17 describes the major loss for an internal flow. The friction factor is a

function of Reynolds number. If the flow is laminar, less than 2300, the friction factor is

described as $64/Re$. If the Reynolds number is greater than 2300, the friction factor is given by Equation 18.

$$h_l = f \frac{L}{D} \frac{\overline{V}^2}{2} \tag{17}$$

$$f = \frac{0.316}{Re^{0.25}} \tag{18}$$

Equation 19 provides the pressure loss due to contraction. For a square-edged nozzle, the minor loss coefficient K becomes 0.5. For high velocities, the minor losses could be significantly larger than the major losses.

$$h_{lm} = K \frac{\overline{V}^2}{2} \tag{19}$$

Table 7 provides the losses from the effusion holes for the case of H/d=1 without ribs. It is clear that the 2mm effusion hole has negligible pressure loss for the system while the 0.5mm and 0.838mm diameters add 24 kPa and 39 kPa respectively.

Table 7- Minor and major losses due to the effusion holes

Pressure Drop across Effusion Hole (kPa)			
Regions	0.5 mm d_{eff}	0.838mm d_{eff}	2mm d_{eff}
Entrance	22.1	37.7	1.2
Length	2.0	1.7	0.0
Total Loss	24.1	39.4	1.2

The pressure calculations then needed to be compared with the simulation data. The pressure drop from inlet to outlet was recorded from each of the 18 simulations. For each H/d and surface geometry, the pressure drop was the same. Table 8 shows this trend. It was then suggested that the pressure drop across the 2mm effusion hole was negligible and the pressure drop of 23 kPa is the losses from the impingement holes and third layer. With this assumption the losses across the 0.5mm and 0.838mm effusion holes were added to the 23 kPa. With this addition it can be concluded that 8 kPa and 17 kPa are the losses due to expansion for the 0.5mm and 0.838 mm effusion holes. It must also be pointed out that the effusion losses were only accounted for one effusion hole. This shows that all the effusion holes are in parallel. The best configuration of effusion holes would provide a large effective area. This means the flow leaving the effusion holes has enough area to result in a small mean velocity. A simple volume flow calculation could be used to find number of holes and at what diameter one would need to negate the pressure loss due to contraction.

Table 8- Pressure drop across the three-layer model

Pressure Drop across model (kPa)						
	w/out Ribs			w/ Ribs		
H/d	0.5 mm d_{eff}	0.838mm d_{eff}	2mm d_{eff}	0.5 mm d_{eff}	0.838mm d_{eff}	2mm d_{eff}
1	55.9	80.7	23.6	57.4	80.8	24.0
3	57.9	78.5	23.1	58.1	78.3	23.2
6	57.6	79.7	23.4	58.0	79.5	23.2

Rectangular (1"x6") Comparisons

The effectiveness of the three-layer design is evident when the heated surface becomes elongated or the span-wise distance of the heated area is very large compared to the jet-to-jet spacing. Three different cooling models will be presented for comparison; an internal parallel flow model, a traditional impingement model, and a three-layer design. For there to be an "apples to apples" comparison the geometries will be identical in almost all dimensions. The three layer model will have an effusion diameter of 2mm, H/d=1, and no ribs on the heated surface. The traditional impingement model will have the same inlet channel dimensions, jet nozzle dimensions, and impingement channel dimensions as the three-layer model for H/d=1. The parallel flow model will have a channel height of 0.838mm or the equivalent of an impingement layer when H/d=1. A mass flow rate was given that for all three models 6 times greater than that of the smaller heated surface models. This is to insure that the jet Reynolds number remains the same for the impingement cases. The same boundary conditions used for the smaller heated model are applied to the rectangular model. The first model to be analyzed is the three-layer model.
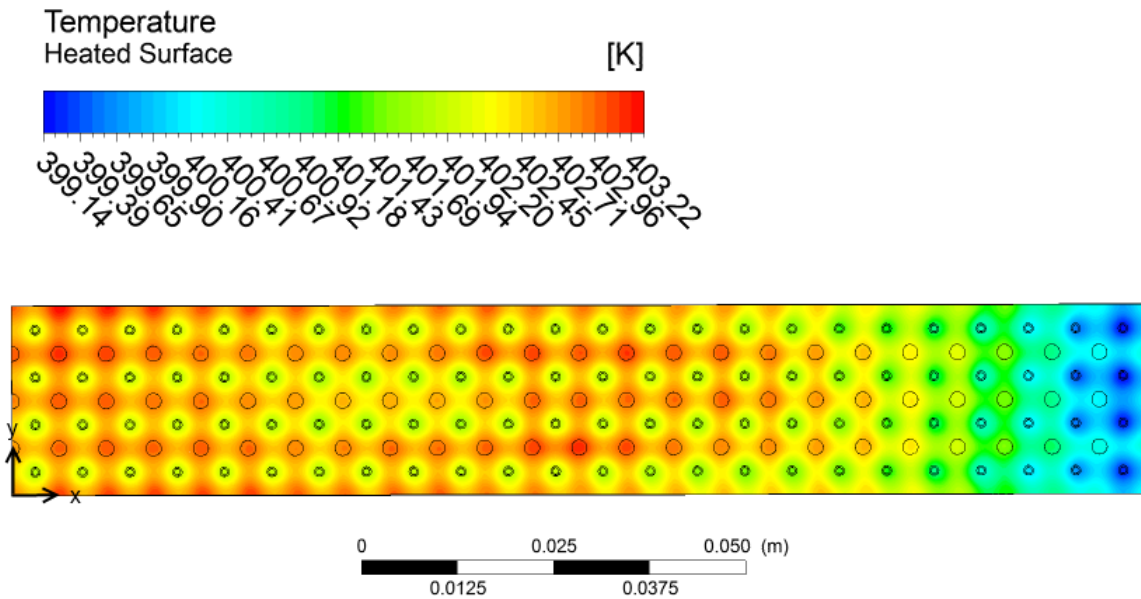
Figure 24- Heated surface temperature plot for a three-layer model

The temperature distribution and average heat transfer coefficient for the elongated model are almost identical to the smaller models with the same parameters. The impingement regions are clearly shown on the surface. There are no signs of cross-flow along the stream-wise direction. There is a noticeable increase in intensity of impingement in the positive stream-wise direction. This is due to the pressure drop that the impingement holes encounter downstream, although it is not nearly as strong as the pressure drop seen in tradition impingement models that experiences cross-flow. Figure 24 highlights the pressure change in the stream-wise direction. Since the effusion holes have negligible pressure drop when the velocity is low, the impingement channel is slightly affected by the pressure drop in the middle layer, hence the non-uniform impingement intensity.
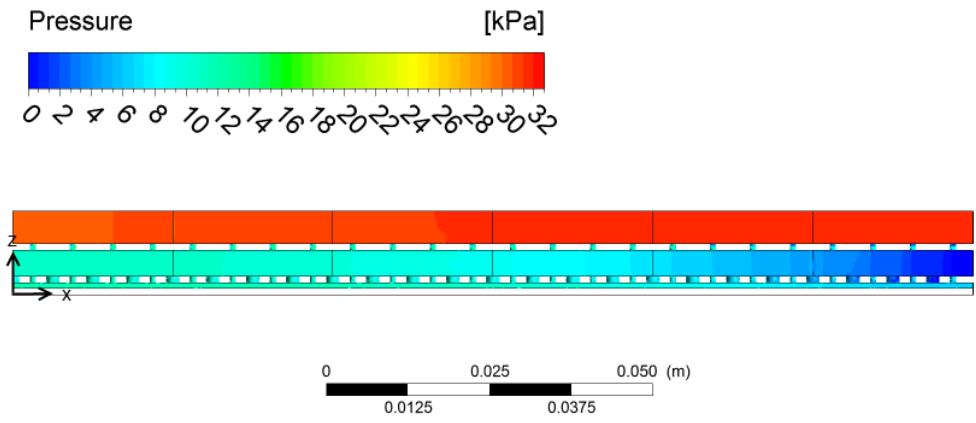
Figure 25- Stream-wise distribution of pressure in the three-layer model

The traditional impingement model suffers greatly from the effects of cross-flow. As stated above, the jet velocities vary along the stream-wise direction because of the pressure change in the impingement channel. This pressure distribution is shown in Figure 25.
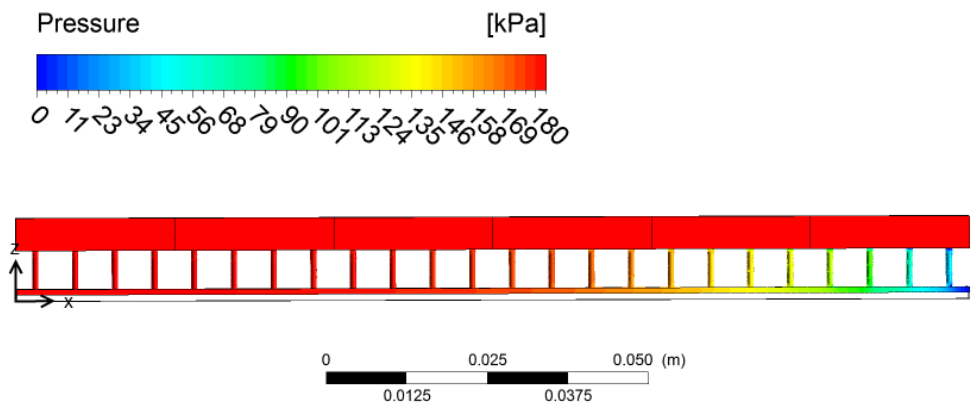

Figure 26- Stream-wise distribution of pressure in the tradition impingement model

This large pressure gradient causes the heat transfer to monotonically increase in the x-direction as the jet velocity increase.
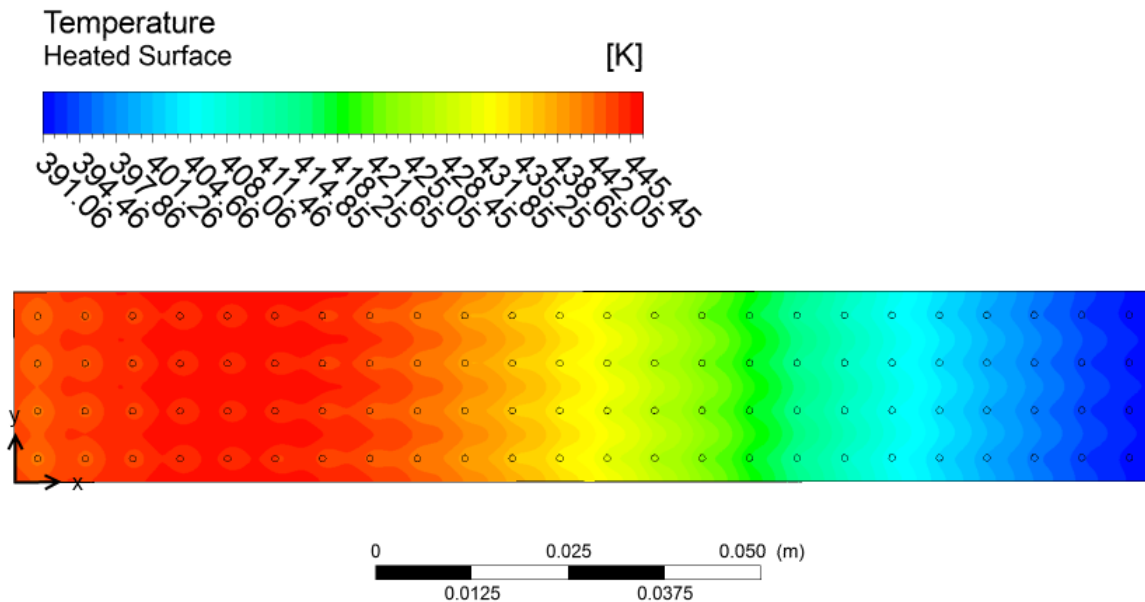
Figure 27- Heated surface temperature plot for the tradition impingement model

This trend of increasing heat transfer coefficient as the span-wise direction increases is shown in Florschuetz when analyzing Nusselt numbers for H/d=1. However, this trend was not seen for H/d=2 or 3. The final comparison model was the parallel flow model. The heat transfer occurring within the small channel displayed a small temperature change on the heated surface, only 2.26°C while maintaining a high heat transfer coefficient. One of the main reasons was due to the high Reynolds number, 14195. The heat transfer for the parallel case was 48% greater than the three-layer model but at the cost of having a pressure loss 6.95 times that of the three layer. The traditional impingement suffered from the cross-flow effects in both pressure loss and heat transfer. The average heat transfer coefficient for the three-layer model was 1.84 times greater than the traditional impingement model while maintaining a pressure loss 83% less than the traditional model. Table 9 show the key values obtained from the results of each of the three simulations.

57

Table 9- Comparison of elongated models when H/d=1

Comparison of 1"x6" models (H/d=1)		Traditional	
	Parallel	Impingement	3 Layer
T_{max} (K)	395.0	446.6	403.3
T_{avg} (K)	392.7	426.4	402.1
T_{min} (K)	392.7	391.1	399.1
ΔT	2.3	55.5	4.2
h_{avg} (W/m^{2}K)	11786.4	4319.8	7950.2
ΔP (kPa)	213.4	187.8	30.7

It should be noted that the pressure drop in both the parallel case and tradition impingement case were extreme and are not satisfactory for the present cooling goals. This comparison simply demonstrates that the three-layer design enhances jet impingement cooling for long surfaces by managing the spent fluid. Traditional impingement is satisfactory until the span-wise distance becomes too great and internal flow becomes expensive to pump through the channel due to the small hydraulic diameter and high Reynolds number needed to have effective cooling. Comparison models are more accurately represented when H/d=3. In these cases the heat transfer for the three-layer model is 2 times greater and 1.75 times greater than the internal parallel model and traditional impingement model, respectively.

Table 10- Comparison of elongated models when H/d=3

1"x6" Traditional models (H/d=3)		Traditional
	Parallel	Impingement
T_{max} (K)	435.4	432.2
T_{avg} (K)	431.2	423.6
T_{min} (K)	430.2	415.5
ΔT	5.2	16.7
h_{avg} (W/m^{2}K)	3960.9	4556.5
ΔP (kPa)	8.8	34.6

<u>Additions</u>

The research up to this point has optimized three-layer jet impingement to traditional impingement. We have seen the benefits that occur for the three-layer model in heat transfer coefficient, temperature uniformity, and pressure drop. But it can also be seen that when comparing the three-layer model to parallel flow, the parallel flow outperformed the three layer model in some categories such as average heat transfer coefficient. To optimize the three layer impingement model to parallel flow, some variables need to be modified to show the advantage of the three layer model, variables that up to this point have not been modified. Some of the variables presented are tailored to this experiment and may need different parameters for other cases but the principles still applies. The first variable changed will be the heat flux imposed on the cooling system. Even though the heat transfer coefficients will not be affected by this change, the differences in temperature uniformity will become clearer. The heat flux will increase by a factor of three, from 23 W/cm^2 to 70 W/cm^2. Another significant variable needing to be modified is the Reynolds number for parallel flow. To do this without changing the geometry of the model or the fluid properties the mass flow will be changed. The goal is to have comparable Reynolds numbers between the internal channel and the impinging jets. Equation 15 provides a basis on what variables affect the non-dimensional heat transfer coefficient for jet impingement. Reynolds number and impinging geometry are the dominating variables for an impinging process that has no cross flow, such as a three layer model. Equation 20 provides the Nusselt number correlation for turbulent flow in a pipe.

$$Nu = 0.023 Re_D{}^{4/5} Pr^{0.4} \tag{20}$$

By this equation, a correlation for heat transfer coefficient to mass flow can be made for internal flow. Then with a mass flow rate reduced to 1/4th, the equation shows that the heat transfer coefficient will be 1/3rd its original value. For the three layer model to maintain its original jet Reynolds number while also having 1/4th the mass flow, a reduction in the number of impinging holes is required. 1/4th the amount of holes are used. Therefore the small geometry that originally had a 4x4 inline jet arrangement will now contain a 2x2 inline jet arrangement. Figure 28 shows the geometric configuration for the modified three layer design. The impingement holes are placed 2x2 with an inline pattern. This leads to double the distance for x/d and y/d. The increase in distance between the impinging holes only reduces the three-layer average heat transfer by one half which will be seen later.
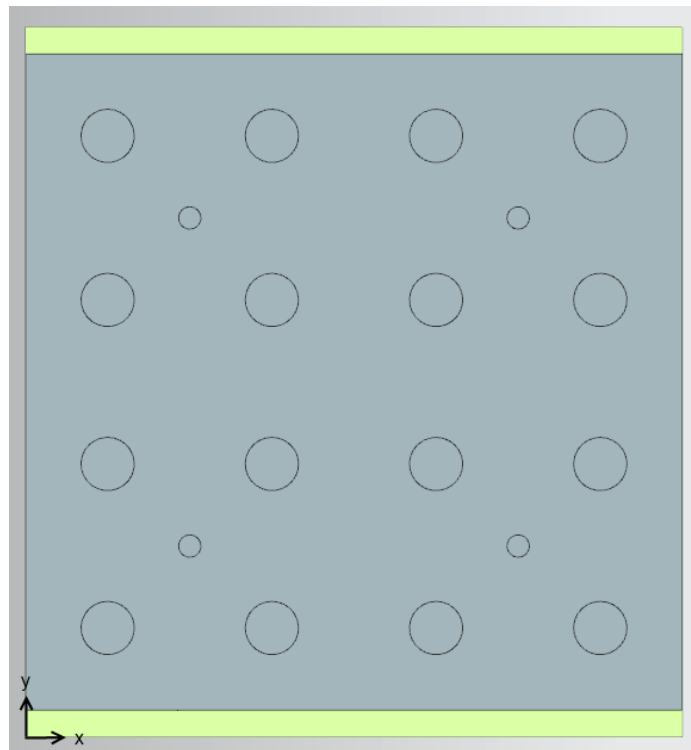

Figure 28 - Effusion plate showing the modified jet holes and effusion holes

The third variable will be the bottom layer thickness. The temperature plots in the previous sections show small temperature changes, 2-10 °C, across the heated surface. This was due to the relatively large flow rate and small heat flux compared to the ones that will be used for this section. To better analyze the affects of bottom surface thickness for parallel and three layer design, bottom thicknesses of 1, 3, and 5 mm will be used.
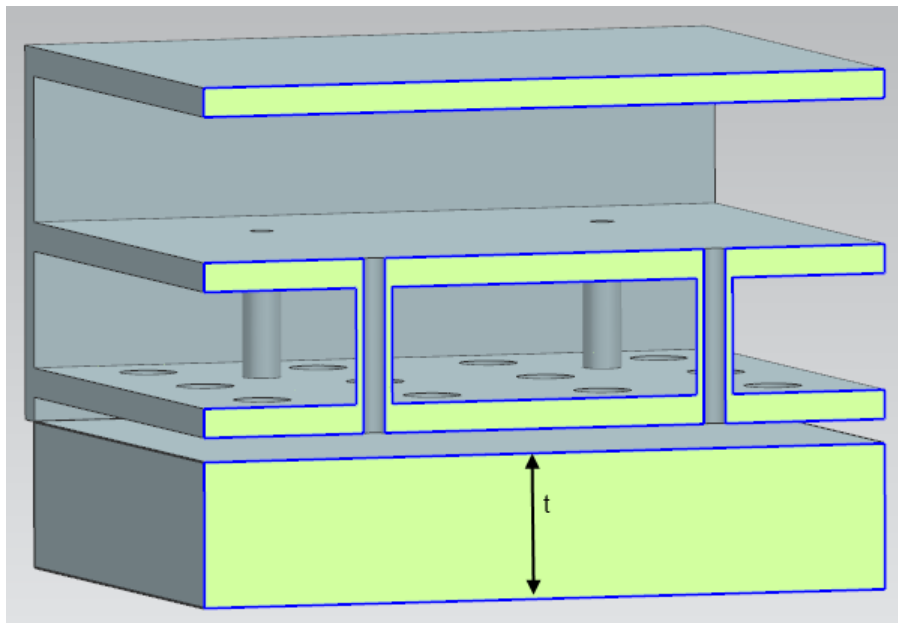

Figure 29 – Three layer design showing bottom layer thickness

The goals for the modified three layer geometry are the same as before; provide a high average heat transfer coefficient, uniform temperature on the heated surface and low pressure loss. But now a direct comparison will be made against the parallel flow case while before the three-layer model was tailored towards tackling the drawbacks of jet impingement with cross flow.

After testing the different H/d impingement cases, it was found that H/d=3 would provide the best heat transfer characteristics for the comparison.   Since the temperature profiles are not uniform in the x and y direction, two points were used to measure from along the y axis. The first was the point of impingement in the y-direction and the second was the midpoint between the impinging jets in the y-direction. These two locations can be seen in Figure 30.
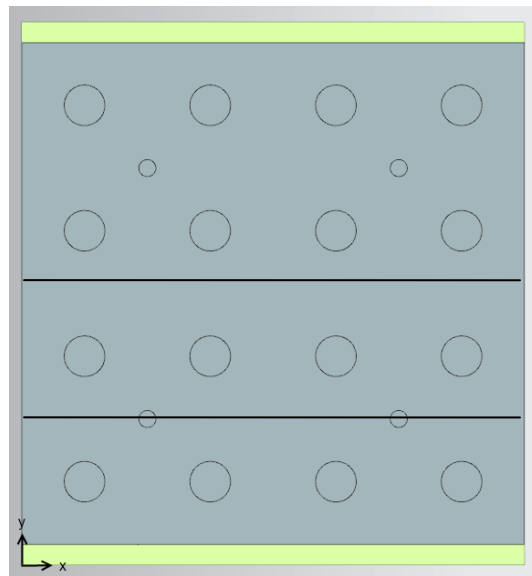

Figure 30 - Effusion plate showing the locations of temperature measurements

With these two locations we were able to record the coldest and hottest temperatures at any given x location. Figure 31 shows the temperature distribution across the length of the elongated heated surface for the impinging model. It can be seen that the temperature difference for a given x-location decreases when the bottom surface thickness is increased. The maximum temperature difference along the x direction for a 1 mm surface thickness was 16.5°C. This difference decreases to 4°C for a 3 mm thickness and even further, 1.4°C difference, for a 5 mm bottom thickness. This decrease does come at the cost of a lower heat transfer coefficient.
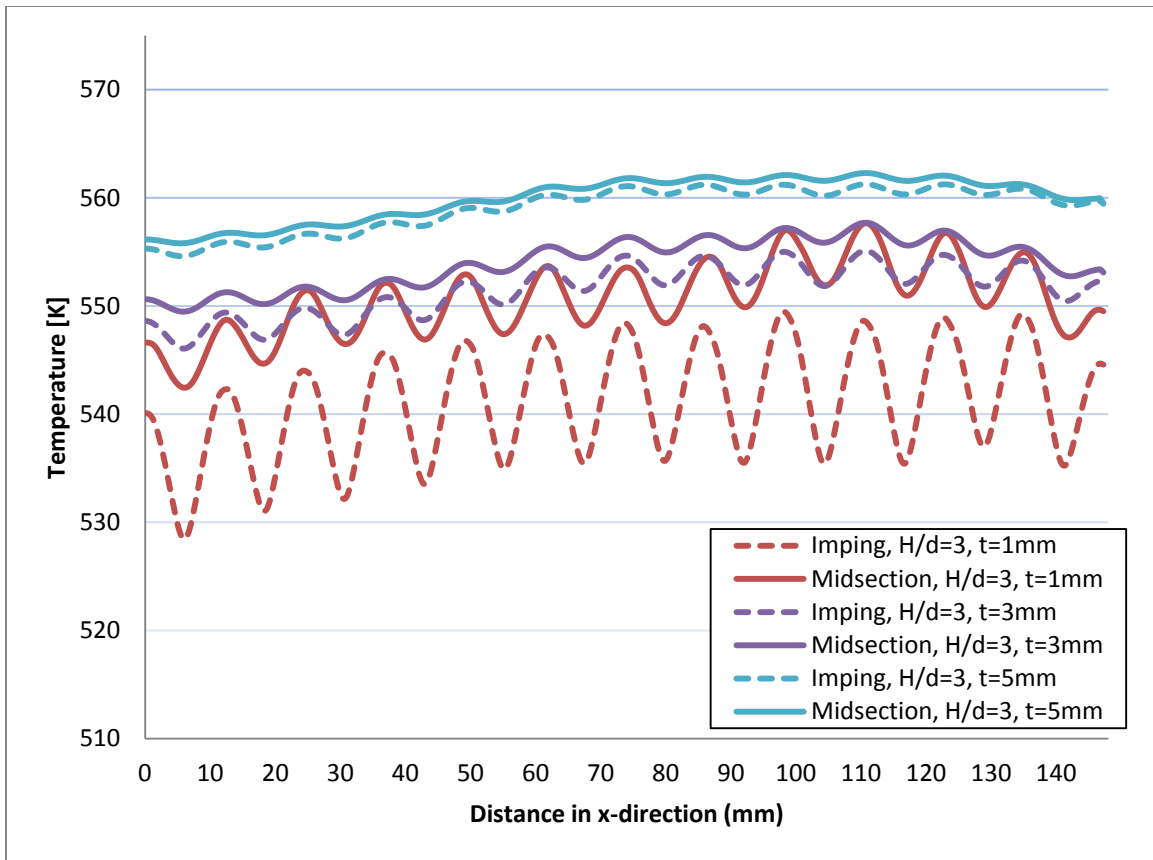
Figure 31 – Temperature distribution of three-layer model over an elongated surface

The parallel flow model H/d=1 showed to be the most the beneficial cooling model and was used to compare against the three-layer model. A temperature profile was recorded and a 1-D plot was taken. This 1-D assumption can be made for the internal flow case since the fluid interacting with the heated surface is uniform in the y-direction i.e. there is no velocity term in the y direction. To compare the three-layer to parallel in a 1-D analysis, the midsection plot was used for the impingement case.
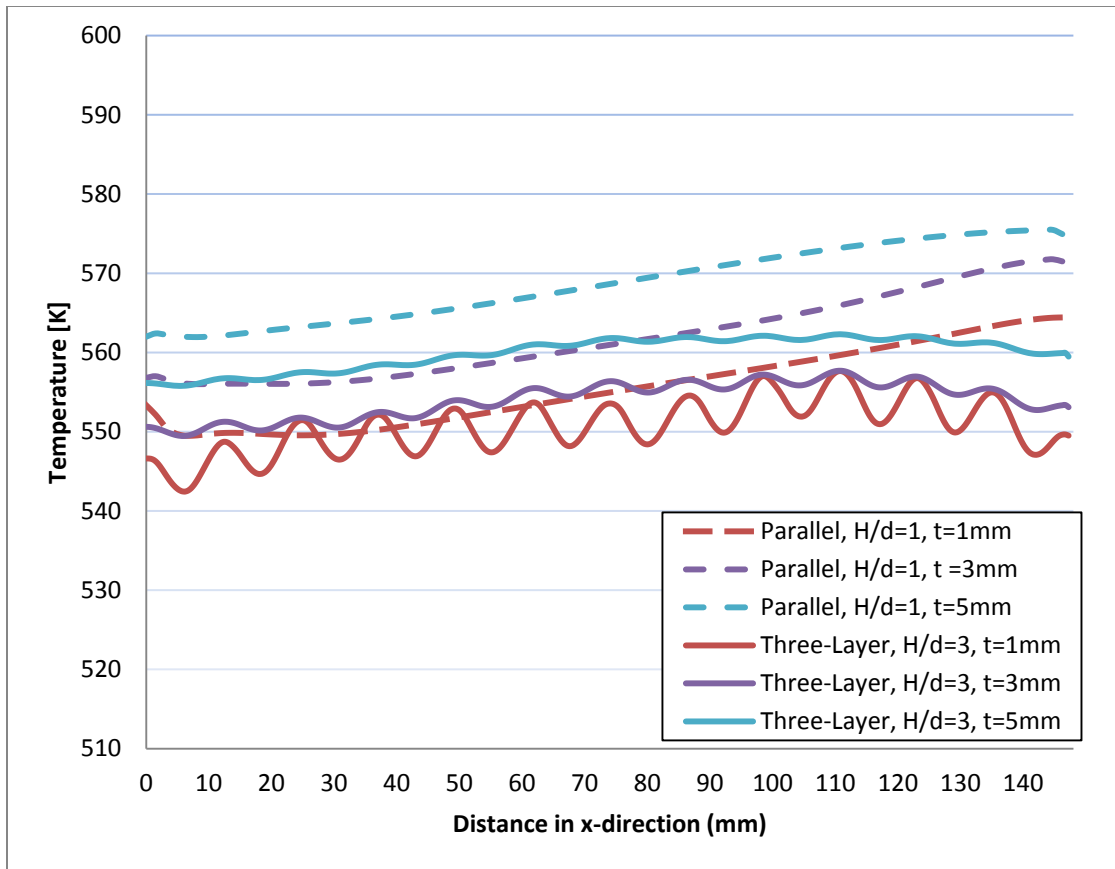
Figure 32 - Temperature distribution for parallel and three-layer models over an elongated surface

Figure 32 shows that the parallel flow temperature increase in the x direction is dependent on the fluid temperature increase which is 19°C for this case. This is mainly due to the concept that once the internal flow reaches a fully developed state the wall temperature will increase at the same rate as the fluid temperature in a linear fashion. The three-layer model is less dependent on the fluid temperature increase and the surface temperatures become more uniform as the bottom surface thickness increases. To take advantage of the parallel flow's

dependence on fluid temperature, one can either raise the heat flux of the design or have a

smaller mass flow rate to take advantage of jet impingement.

After looking at the temperature uniformity on the surface, a look at the average heat

transfer coefficient is necessary. As mentioned earlier, the changes in mass flow rate affected

the average heat transfer coefficient for both the parallel and three-layer models. It can be seen

in Table 11 that the three-layer model, which before was 50% less than the parallel flow, is now

5% better. This benefit exists for all thickness used.

Table 11- Average heat transfer coefficients for modified design

Avg. heat transfer coefficient (W/m²K)		
	Parallel	Three-Layer
t = 1 mm	3831.6	4055.7
t = 3 mm	3707.4	3899.2
t = 5 mm	3579.6	3757.2

The three-layer model could be modified even further to a single jet as compared to the

2x2 arrangement that is presently used. If the same process of reducing mass flow rate is used,

the three-layer model would only decrease by one half while the parallel flow model would be

reduced to 1/3 the values shown in Table 11. The reduction in flow rate would also produce a

laminar flow within the parallel model leading to a further reduction in heat transfer.

In terms of pressure drop, for the three-layer 2x2 arrangement and parallel flow models,

the pressure loss is between 17 - 21 kPa. The pressure loss for the three-layer model could be

reduced even further if round inlets are used for each of the impinging nozzles. This would

reduce the minor loss coefficient for pipe entrances but not the contraction or expansion

coefficients.

The accuracy and reliability of the present research must be tested and compared against experiments that have been accepted in industry as well as scholarly journals. Without any validation to the simulations the results hold no foundation and would not be accepted among journals or other technical papers in the field of study. Especially with simulations, experimental data is needed to uphold the results. Florschuetz et al. [12] provides an extensive study on jet impingement and will be used as a source to validate the results from this research. The main goal is to prove that the numerical model and simulation setup would accurately describe the fluid flow and heat transfer. Two impingement models were created that fit within the parameters of the correlations provided by Florschuetz, similar to the baseline impingement model. The comparison model had a 24.62mm x 73.86mm (1"x3") heated surface with a 0.838mm diameter jet nozzle spaced 6.15mm apart within an inline formation. An H/d of 2 and 3 were modeled, both of which fit well into the correlation presented. The major parameters used in the setup of mesh and boundary conditions are carried into these models.

The first comparison conducted from the experiments of Florschuetz et al. [12] and the numerical simulations was the stream-wise distribution of jet velocities. A jet velocity distribution model was derived based on the span-wise distance, jet-to-target height and channel length. This distribution was plotted for H/d of 2 and 3. Figure 27 shows the jet velocity distribution normalized by the average jet velocity for the model data and the simulations.
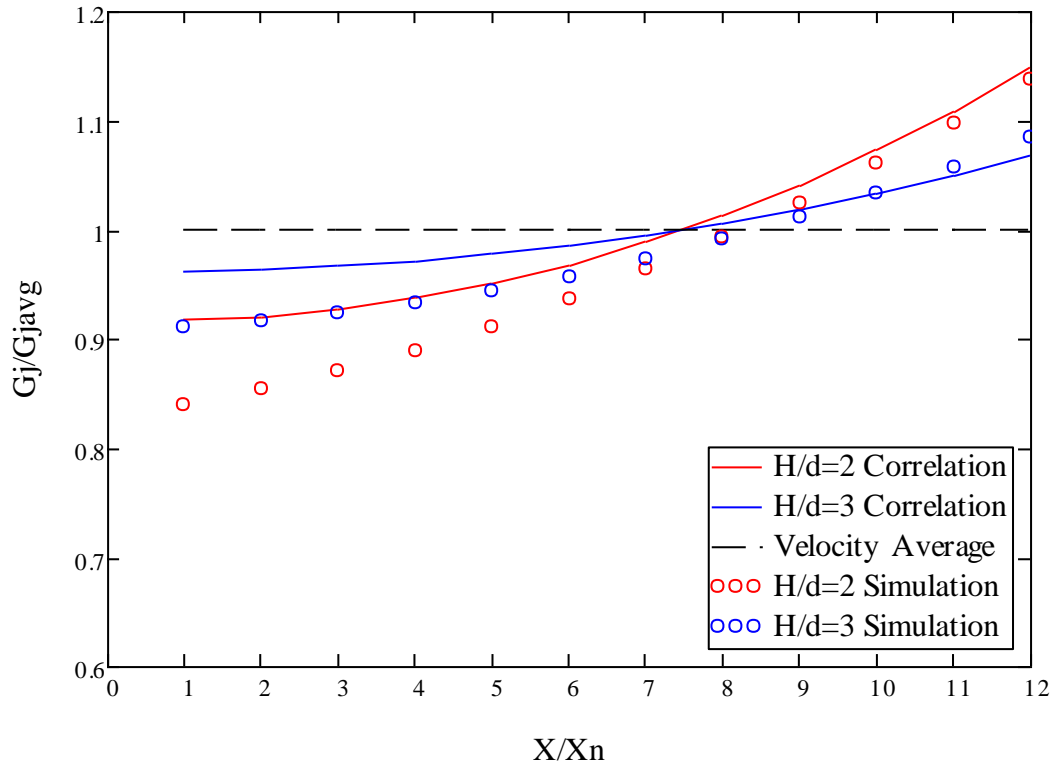
Figure 33- Stream-wise distribution of jet velocities
Comparison between simulated values and model

Jet velocities were measured at the each stream-wise row. Since each nozzle had a turbulent profile, an average was taken over the 2-D profile. The velocities were plotted and a third order polynomial trend line was fitted to the three points, one equation per H/d. These two equations were plotted with the model. For both H/d of 2 and 3 the maximum difference was 8.5% and 5.3% respectively. For H/d of 2 and 3 the average difference of the jet velocities from the model over the whole channel length was 4% and 2.9%, respectively.

Table 12- Jet velocity difference between the simulation and correlation models

G_j/Gj_{avg} error (%)		
x/x_n	H/d=2	H/d=3
1	8.5	5.3
2	7.3	4.9
3	6.2	4.5
4	5.1	4.1
5	4.2	3.5
6	3.3	2.9
7	2.6	2.3
8	2.0	1.6
9	1.5	0.8
10	1.2	0.1
11	1.0	0.8
12	0.9	1.6
AVG	**4**	**2.9**

The plot shows that the simulation effectively predicted the jet velocities of the long channel. Since these velocities are based on the pressure at the inlet and outlet of the jet nozzles, it also accurately predicted the pressure distribution in the bottom layer or impingement region. The final conclusion deduced from this comparison is that the inlet channel height is sufficient large enough to neglect any pressure drop occurring across the 1st layer when calculating the jet velocities. The 1st layer is essentially acting as an inlet plume.

The second comparison conducted from the experiments of Florschuetz et al. [12] and the simulations of the present research is the heat transfer occurring at each stream-wise row of impingement. Specifically, the average Nusselt number at each stream-wise row is to be compared. The correlation model used for comparison was previous given in the present

research in detail. For the purpose of this research plots were given for H/d of 2 and 3. While

the correlation has the ability to model an impingement design with H/d=1, it is proposed that

overall the correlation appears to do an excellent job for H/d = 2 and 3 and an adequate job for

H/d = 1. Therefore H/d = 2 and 3 will only be used for comparison. Figure 34 shows the

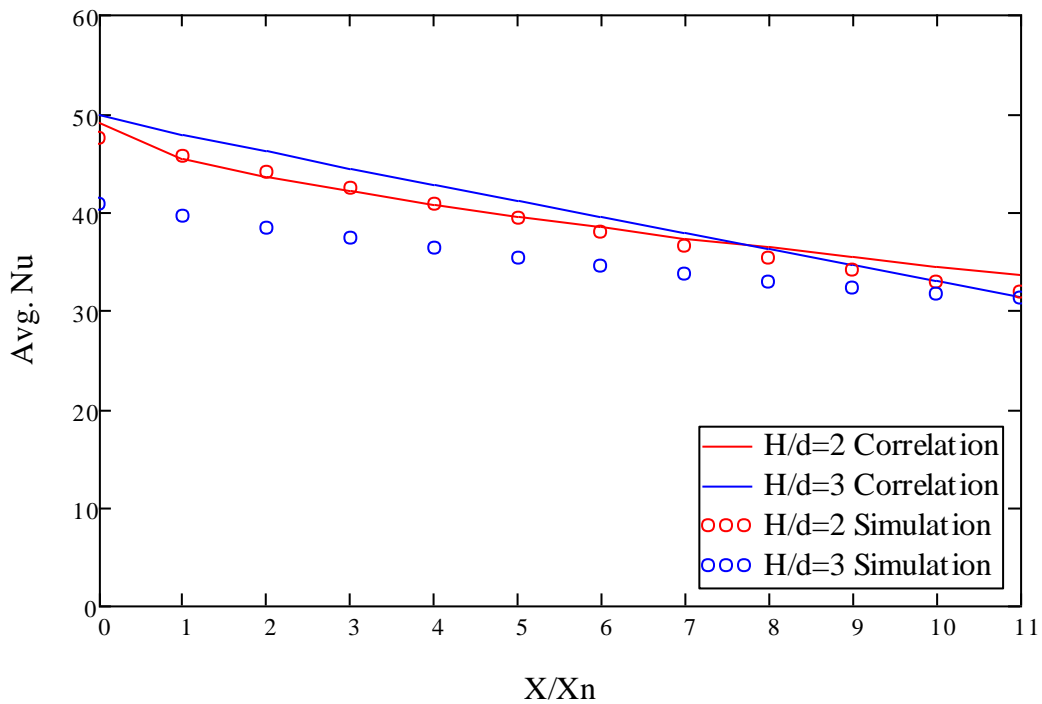stream-wise distribution of Nusselt number for the correlation and simulation data.

Figure 34- Heat transfer correlations compared with numerical simulation data

It must also be mentioned that the test setup only recorded the average Nusselt number at

each stream-wise row. A copper plate, used as the heated surface, created a one-dimensional

thermal profile leaving little to no variance in the span-wise, y, direction. While this simplified

the experiment such was not the case when simulations were conducted. The heated surface was

not assumed to be one-dimensional and therefore requiring the Nusselt number to be averaged in

the span-wise direction for comparison to be accurate with the correlation. 24 measurement

points were taken along the stream-wise direction.

Table 13- Nusselt number difference between simulation and correlation models

Nusselt number error (%)		
X/Xn	H/d=2	H/d=3
1	3.0	18.1
2	0.5	17.4
3	0.8	16.8
4	0.5	16.1
5	0.1	15.2
6	0.8	14.1
7	1.6	12.7
8	2.4	11.1
9	3.2	9.1
10	4.0	6.8
11	4.7	4.0
12	5.3	0.8
AVG	**2.4**	**12.9**

For H/d=3 the maximum difference from the correlation was 18.1%. This occurred at the

midsection of the channel, at the 1st stream-wise row. The average difference across the whole

channel was 12.9%. For H/d =2 the maximum difference from the correlation was 5.3%. This

occurred at end of the channel, at the 12th stream-wise row. The average difference across the

whole channel was 2.4%.

CHAPTER 5 - CONCLUSION

Cooling techniques for high density electronic devices will always be in demand. A

collective effort by many researchers has given the industry a fair understanding of many cooling

models over the past several years but new techniques are being made aware of every year. It

was the goal of this research to find an effective cooling technique, one that combines low cost,

high heat transfer, and low maintenance. The objective was to understand and implement a fresh

approach to jet impingement cooling. The use of effusion holes and heated surface ribs, while

not new, are still young in development for jet impingement. With the aid of numerical

simulation, models were created hoping to find trends in each variable that would lead us to

understand how each one would affect the fluid flow and heat transfer. With a limited amount of

resources, assumptions were made on what ranges would be needed to make correlations from

the results to be in the realm of credible. Over 18 simulations were conducted using reliable

commercial software popular in the CFD field. The numerical models were bounded and formed

by a turbulence model and meshing that was proven accurate for jet impingement [16]. The

numerical model was tested and successfully replicated the experiments provided by Florschuetz

et al. [12]. Boundary conditions were then given to the models that were comparable to real

world scenarios in the industry.

Given the results from the 18 small models and several elongated models, it can be

concluded that a three-layer model effectively managed the working fluid in cases where

traditional jet impingement would develop unacceptable heat transfer effects. Other models

were also able to show how the three-layer model could be used as an effective substitute to

parallel, internal flow. The use of effusion holes and a separate outlet channel allowed the fluid to impinge on the heated surface without significant interaction between jets. For large values of H/d, the fluid showed signs of mixing in the impingement channel while smaller values showed little to no jet interaction in the impingement region. The smaller H/d values also produced the better heat transfer with no change in pressure. When analyzing the effects of effusion hole arrangement, it seemed the heat transfer coefficient was most positively affected when the most effusion holes were present and the pressure loss was least when the effective area of the holes was greatest. Additional research could be done for varying span-wise heated surfaces and its effect on effusion holes. The use of ribs increased heat transfer for every case. It is not known if the ribs were optimized for the current testing or by which means the ribs increased the heat transfer; by guiding the flow of the spent fluid to the effusion holes or by merely acting as fins on the heated surface. While this research did not cover all conceivable flow rates or impingement configurations it can be concluded that a three-layer cooling design is a credible improvement over jet impingement cooling.

APPENDIX - COPYRIGHT PERMISSIONS

IEEE Copyright Permission

Thesis / Dissertation Reuse

The IEEE does not require individuals working on a thesis to obtain a formal reuse license, however, you may print out this statement to be used as a permission grant:

Requirements to be followed when using any portion (e.g., figure, graph, table, or textual material) of an IEEE copyrighted paper in a thesis:

1) In the case of textual material (e.g., using short quotes or referring to the work within these papers) users must give full credit to the original source (author, paper, publication) followed by the IEEE copyright line © 2011 IEEE.
2) In the case of illustrations or tabular material, we require that the copyright line © [Year of original publication] IEEE appear prominently with each reprinted figure and/or table.
3) If a substantial portion of the original paper is to be used, and if you are not the senior author, also obtain the senior author's approval.

Licensed content title	Prandtl-number effects and generalized correlations for confined and submerged jet impingement
Licensed content author	Chin-Yuan Li,Suresh V. Garimella
Licensed content date	September 2001
Licensed content volume number	44
Licensed content issue number	18
Number of pages	10
Start Page	3471
End Page	3480
Type of Use	reuse in a thesis/dissertation
Portion	figures/tables/illustrations
Number of figures/tables/illustrations	1
Format	both print and electronic
Are you the author of this Elsevier article?	No
Will you be translating?	No
Order reference number	
Title of your thesis/dissertation	Heat/Mass Transfer of Three-Layer Impingement/Effusion Cooling System
Expected completion date	Dec 2012
Estimated size (number of pages)	70
Elsevier VAT number	GB 494 6272 12
Permissions price	0.00 USD
VAT/Local Sales Tax	0.0 USD / 0.0 GBP
Total	0.00 USD

REFERENCES

[1]   A. E. King, "SPRAY COOLED GENERATORS AND DESIGN-TO-COST AT WESTINGHOUSE," *SAE Preprints,* 1973.

[2]   D. R. Basel, "NON-CLOGGING NOZZLE FOR ROTATING EQUIPMENT SUCH AS FOR COOLING DYNAMO-ELECTRIC MACHINES," U.S. Patent No. 3659125, 1972.

[3]   R. J. Kennett, "Integrated drive generators for aircraft," *Electronics and Power. Journal of the Institution of Electrical Engineers,* vol. 17, pp. 73-6, 02/ 1971.

[4]   R. GASPERETTI, "Aircraft generator weight reduced by more effective cooling(Spray oil cooling to reduce aircraft generator weight, enhance reliability and lengthen overhaul intervals)," *WESTINGHOUSE ENGINEER,* vol. 29, pp. 71-75, 1969.

[5]   M. Schoning and D. Walti, "Modern PWM drives and high speed machines," in *2011 IEEE International Electric Machines & Drives Conference (IEMDC), 15-18 May 2011*, Piscataway, NJ, USA, 2011, pp. 624-9.

[6]   E. Liebermann, "Rotor cooling arrangement," ed: Google Patents, 2003.

[7]   K. P. J. Doherty, E. W. Down, W. M. Scherzinger, D. E. Stout, and S. L. Waddell, "High speed generator with integrally formed rotor coil support wedges," ed: Google Patents, 2004.

[8]   H. Martin, "Heat and mass transfer between impinging gas jets and solid surfaces," *Advances in heat transfer,* vol. 13, pp. 1-60, 1977.

[9]   F. P. Incropera, T. L. Bergman, A. S. Lavine, and D. P. DeWitt, *Fundamentals of heat and mass transfer*: Wiley, 2011.

[10]   M. R. Pais, J. E. Leland, W. S. Chang, and L. C. Chow, "Single-phase heat transfer characteristics of submerged jet impingement cooling using JP-5," in *Proceedings of the Intersociety Conference on Thermal Phenomena in Electronic Systems, May 4, 1994 - May 7, 1994*, Washington, DC, USA, 1994, pp. 178-183.

[11]   L. Chin-Yuan and S. V. Garimella, "Prandtl-number effects and generalized correlations for confined and submerged jet impingement," *International Journal of Heat and Mass Transfer,* vol. 44, pp. 3471-80, 2001.

[12]   L. W. Florschuetz, D. E. Metzger, and C. R. Truman, "JET ARRAY IMPINGEMENT WITH CROSSFLOW-CORRELATION OF STREAMWISE RESOLVED FLOW AND HEAT TRANSFER DISTRIBUTIONS," *NASA Contractor Reports,* 1981.

[13]   T. J. Bland, R. E. Niggemann, and M. B. Parekh, "COMPACT HIGH INTENSITY COOLER (CHIC)," in *13th Intersociety Conference on Environmental Systems.*, San Francisco, CA, USA, 1983, pp. SAE, Warrendale, Pa, USA.

[14]   D. H. Rhee, J. H. Choi, and H. H. Cho, "Heat (mass) transfer on effusion plate in impingement/effusion cooling systems," *Journal of Thermophysics and Heat Transfer,* vol. 17, pp. 95-102, 2003.

[15]   T. B. Hoberg, A. J. Onstad, and J. K. Eaton, "Heat transfer measurements for jet impingement arrays with local extraction," *International Journal of Heat and Fluid Flow,* vol. 31, pp. 460-467, 2010.

[16]   N. Zuckerman and N. Lior, "Jet impingement heat transfer: physics, correlations, and numerical modeling," *Advances in heat transfer,* vol. 39, pp. 565-631, 2006.

[17]   G. Kalitzin, G. Medic, G. Iaccarino, and P. Durbin, "Near-wall behavior of RANS turbulence models and implications for wall functions," *Journal of Computational Physics,* vol. 204, pp. 265-91, 03/20 2005.

[18]   W. M. Kays, *Convective heat and mass transfer [by] W.M. Kays*. New York: McGraw-Hill, 1966.

[19]   N. K. Chougule, G. V. Parishwad, P. R. Gore, S. Pagnis, and S. N. Sapali, "CFD analysis of multi-jet air impingement on flat plate," in *World Congress on Engineering 2011, WCE 2011, July 6, 2011 - July 8, 2011*, London, United kingdom, 2011, pp. 2431-2435.

[20]   T. Peng, L. Qing, and X. Yimin, "Investigation on the submerged liquid jet arrays impingement cooling," *Applied Thermal Engineering,* vol. 31, pp. 2757-63, 10/ 2011.

[21]   R. W. Fox, A. McDonald, and P. Pitchard, "Introduction to Fluid Mechanics," ed: John Wiley & Sons, Inc, 2006.